Development and Assessment of a Blade Element Momentum Theory Model for High Solidity Vertical Axis Tidal Turbines.

Brian Mannion [1,*], Seán B. Leen[1,*], and Stephen Nash [1,*]

[1] College of Engineering & Informatics, National University of Ireland Galway, Ireland and SFI Centre for Marine Renewable Energy Ireland.
***** Correspondence: b.mannion4@nuigalway.ie; stephen.nash@nuigalway.ie

ABSTRACT: Tidal energy is an attractive renewable resource given its predictability. The production of reliable, efficient and cost-effective tidal energy turbines requires the development of computer models for assessment and design optimisation of turbine performance. Blade element momentum theory (BEMT) models are attractive to turbine designers as they have a very low computational cost compared to CFD models. In this paper, we develop a BEMT model for high solidity and highly loaded vertical axis tidal turbine rotors which traditional BEMT models are incapable of modelling. The double multiple stream-tube model employs a graphical approach for determination of axial induction factors rather than the iterative approach used in traditional BEMT models. Corrective methods to account for dynamic stall, flow expansion, and finite aspect ratios are also implemented in the model. Model performance is assessed against experimentally measured power performance data of both low and high solidity rotors. The model reproduced peak efficiency values to within 2.5 % for a low solidity wind turbine, 8 % for a high solidity wind turbine and to within 10 % for a high solidity tidal turbine in confined flow.

KEYWORDS: Blade element momentum theory; Double multiple stream-tube; High Solidity; Vertical axis tidal turbine; Performance prediction.

1. Introduction

Experimental testing [1–5] is regarded as the gold standard in the performance analysis of turbines. However, the cost associated with testing can be prohibitive to early stage developers and access to suitable testing facilities may also be problematic due to their sparse numbers; numerical models therefore play an important role in turbine design and development. Blade element momentum theory (BEMT) models are widely used for early stage development of both tidal and wind turbines, e.g. [6–10]. They model the power performance of a turbine based on the rotor aero-/hydrodynamics and are, therefore, suited to the investigation of the effects of design changes on power performance. They are significantly less computationally compared to CFD [11,12] and can usually achieve a satisfactory level of accuracy for evaluation of design iterations. BEMT combines blade element theory with momentum (actuator disc) theory. In its simplest form, actuator disc theory involves application of 1D linear momentum theory along a single stream-tube enclosing the turbine rotor, with the rotor represented as a porous disc. Blade element theory involves dividing the blades into non-interacting elements and subsequently calculating the forces on each element from lift and drag data for the blade section. The change in fluid momentum due to interaction with a turbine rotor causes a decrease in fluid velocity which is described by the axial induction factor, a, defined as the fractional decrease in fluid velocity caused by the presence of a turbine rotor. BEMT models use momentum theory to help determine the induced velocities which then generate the forces on the blade elements based on their lift/drag characteristics. Accurate

determination of the local axial induction factor and specification of foil lift and drag data are thus key components of any BEMT model.

BEMT was first introduced for propellers by Glauert [13]. Templin [14] was the first to adopt the approach for vertical axis (wind) turbines (VATs) through the development of a single stream-tube model where the turbine was modelled as a single actuator disc enclosed within a single stream-tube (Figure 1 (a)). Templin's approach for VATs was extended by Strickland [15] by dividing the single stream-tube into aero-/hydrodynamically independent multiple stream-tubes to create the single multiple stream-tube model (Figure 1 (b)). The use of multiple stream-tubes allows one to model variations in the axial induction factor across the turbine. While the single multiple stream-tube model can be applied to both horizontal and vertical axis turbines, it cannot account for the induction of velocity between the upstream and downstream of a VAT. The model, therefore, assumes a symmetrical relationship between the loads upstream and downstream. A solution to this problem is achieved by placing two actuator discs in tandem to create the double multiple stream-tube model (DMST) [16–18] shown in Figure 1 (c). The DMST model allows separate analysis of the upstream and downstream halves of the rotor; thus enabling the variation of induced velocity between the upstream and downstream of the rotor to be modelled.

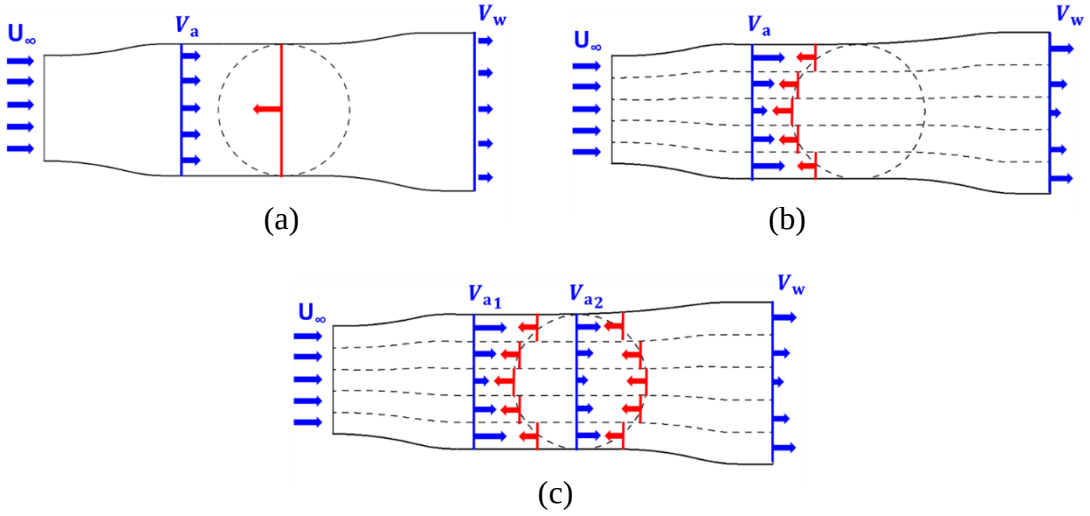

Figure 1: Stream-tube model variations: (a) Single steam-tube model, (b) Single multiple stream-tube model, (c) Double multiple stream-tube (DMST) model with varying induction factor. Blue arrows indicate fluid velocities; red arrows indicate forces exerted on the fluid by actuator disc.

A key step in BEMT model codes is the calculation of the local axial induction factor for each stream-tube; historically this has proven to be very difficult for vertical axis tidal turbines (VATTs) as they have high solidities. Nearly all BEMT models developed to date have relied on Strickland's iterative approach to determine the local axial induction factor for a stream-tube. The iterative approach involves an initial guess for a, which is subsequently used to calculate the blade element forces. The a value is then recalculated, as are the forces, and this procedure continues until a specified convergence criterion is reached and the a value is deemed to be converged. For high solidity / highly loaded rotors, e.g. VATTs, the iterative approach can lead to problems such as erratic solutions and convergence failures [15, 19–21].

The use of a relaxation factor can improve the model but does not eradicate these issues. As an alternative, McIntosh *et al.* [22] developed a graphical approach for determination of the local induction factor suitable for high solidity / highly loaded rotors. For each stream-tube, the force coefficients for the momentum and blade element models are graphed for a range of a values (-1 to +1) and the point of intersection of the two graphed lines, i.e. the crossing point, indicates the appropriate induction factor. McIntosh *et al.* also provide a method for dealing with cases where there are multiple crossing points which they report are caused by stall and hypothesise are the cause of the convergence issues associated with the iterative approach. Stall results in a sharp drop in the applied stream-wise force coefficient which in turn results in multiple intersections between the blade-element and momentum models.

Over the years, many researchers have contributed methods for dealing with identified shortcomings in BEMT models to improve their accuracy. Most of these methods attempt to correct the models for processes that have been omitted or simplified in the underlying theory. Read and Sharpe [5, 12] pioneered the flow expansion correction approach for VAWTs to enable their DMST to account for the stream-tube expansion that occurs between the upstream and downstream actuator discs due to conservation of mass. This stream-tube expansion is of interest for VATTs as it is most significant in the cases of highly loaded rotors. Paraschivoiu *et al.* [23] consider an alternative approach for flow expansion based on sudden expansion, where the azimuthal angle is used in the calculation as opposed to the definition of a new angle by Read and Sharpe.

Dynamic stall is an erratic nonlinear anomaly, primarily caused by the rapid change in the angle of attack of a foil, which can result in a significant loss in lift due to flow separation. The stall angle of a rotating foil is different to that of a static foil [24] and as BEMT models typically utilise static foil data corrective approaches have been developed to account for their use. Paraschivoiu [25] provides a detailed overview of stall models that have been adapted for VATs. The Gormont model [26], with modifications by Massé [27] and Berg [28], is widely implemented in BEMT codes for VATs as it can be easily incorporated. Alternatively, there is the Leishman–Beddoes model, developed by Beddoes [29] and modified by Leishman *et al.* [30], which models the attached and separated flow conditions. However, both approaches have been shown to exhibit discrepancies in comparison to experimental data for normal and tangential coefficients [31]. It should be noted though that these discrepancies may be because other processes are not being modelled correctly within the BEMT model.

Secondary flow effects such as flow curvature and strut effects can also potentially affect the performance prediction capabilities of BEMT models. The two-dimensional circular motion of a vertical axis turbine blade aerofoil may be decomposed into a translational movement and a constant pitching motion. The effects of the pitching motion are usually referred to as flow curvature effects [47], Oftentimes, the pitching motion is overlooked or, when it has been considered, its impact has not been fully accounted for or has even been misinterpreted. Coiro et al. [47] accounted for the effects of the pitching motion of the blade in their model by adding an estimation of an equivalent additional angle of attack; however, the use of this added angle of attack approach is only valid if the circulation term is solely dependent on the pitch rate, and not on a fixed added angle of attack. A comprehensive investigation carried out by Ferreira [37] shows that although flow curvature affects the pressure distribution of the blade, it has negligible effects on power extraction.

Some recent studies have investigated the parasitic effects of the horizontal support struts of

VATs on turbine performance. Using a 3D URANS CFD model, Mannion et al. [12] investigated strut effects for a scale model high solidity rotor and found that the modelled turbine power coefficients were noticeable lower with the struts in place compared to a model with no struts and that the strut effects increased with tip speed ratio. Kirke and Paillard [48] also show that strut effects can have a significant effect on turbine rotor performance and present a method to account for these effects in a BEMT model. De Marco et al. [50] investigated the potential for reducing the parasitic effects of struts by using inclined, rather than horizontal, struts instead of the more conventional horizontal struts. Although their CFD study concluded that inclined support struts can actually contribute to performance they do not present any quantitative comparison to model scenarios with horizontal support struts.

A further problem relating to the foil lift and drag data used in BEMT models, e.g. the Sheldahl and Klimas dataset [32], is that they are typically determined for blades of infinite length. Some researchers have looked at the development of corrective approaches for the use of infinite length blade data for finite length blades. When the angle of attack is less than the static stall angle, Lanchester-Prandtl theory [33] is used to make this correction. When the angle of attack exceeds the stall angle the corrective approach developed by Viterna and Corrigan [34] and modified by Castelli *et al.* [35] is used.

Although the majority of published BEMT models are used to inform initial design decisions and, therefore, generally omit comparisons to experimental performance data, there are some studies which do evaluate the model accuracy. The following are some examples for VATs. Strickland's BEMT model [15] of the SANDIA 17 m Darrieus turbine was shown to relatively accurately predict the peak performance and overall shape of the power curve. The model did over-predict the turbine's performance over the full range of the power curve but the error in peak performance was only in the range of 5 to 10 %. Castelli *et al.* [35] also assessed the accuracy of their BEMT model against the same experimental data. The model included dynamic stall, finite aspect ratio correction and a sudden flow expansion correction for the downstream portion of the azimuthal cycle. The model accurately predicted peak performance (within 5 %) but significantly over-predicted performance levels above the optimum tip speed ratio (λ_{opt}). Finally, Soraghan [36] assessed their BEMT model accuracy for the VAWT 450, a wind turbine of 450 m^2 frontal area. The model over-predicted peak performance by between 12 to 15 % and there was a phase shift in the power curve with optimum peak performance predicted to occur at a λ value of approximately 4 instead of the measured value of 3.

This paper presents the development of a DMST BEMT model for prediction of the hydrodynamic performance of high solidity and highly loaded vertical axis tidal turbines. The model uses the graphical approach for determining induction factors developed by McIntosh *et al.* [22], rather than the more common iterative approach. To the author's knowledge, this is the first time this approach has been applied to VATTs. This is significant because the traditional iterative approach is not usable for high solidity turbines. Corrective methods for flow expansion, finite aspect ratio and dynamic stall are implemented in the model and can be switched on and off for simulations. With regard to secondary flow effects, because of its documented negligible impact on power performance flow curvature was ignored but a correction for the effects of blade support struts on power performance was included. There is very little published literature on the implementation of the graphical approach in BEMs, particularly along with any corrective methods, or on the assessment of the performance of such models for high solidity rotors, and there are no such studies for VATTs. The research therefore makes an important and new contribution to knowledge in these areas. For a VAT, Reynolds number can vary significantly around the azimuthal rotation; the developed BEMT

model captures this by recalculating Reynolds numbers for each blade element location and for every potential induction factor. The accuracy of the BEMT model is assessed by comparing modelled power coefficients with published measured data from both low and high solidity VATs.

2. Model Description

The model presented here is a DMST for VATs created within MATLAB. It was developed for high solidity / highly loaded vertical axis tidal turbines, but it is also applicable to low solidity rotors and wind turbines. The following sections present the underlying theory of the model, an overview of its structure and solution procedure, and short discussions of the representation of the turbine within the model, the requirement for lift and drag coefficient input data and the types of model output.

2.1. Actuator Disc (Momentum) Model

In the model, the turbine is represented as two consecutive actuator discs in tandem which are located at the upstream and downstream faces of the turbine. This is shown in Figure 2 for a single stream-tube structure which is only used here for ease of explanation. All flow enters at the inlet and exits at the outlet of the stream-tube. The presence of the actuator disc causes a pressure discontinuity in the fluid passing through the stream-tube. Actuator disc model theory is based on the following key assumptions:

- The flow is steady-state, homogenous, and incompressible.
- There is no frictional drag exerted by the disc/turbine.
- The thrust over the disc or rotor area acts uniformly within that disc or tube.
- The turbine wake is non-rotating.
- The static pressure far upstream and far downstream of the rotor is equal to the free-stream pressure.

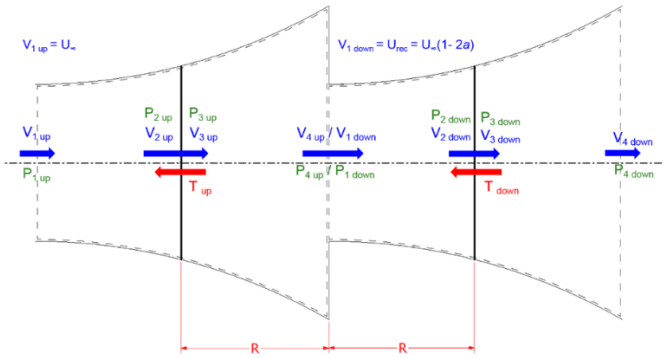

Figure 2: Schematic of a single stream-tube, double actuator disc model used for VATs showing two discs / control volumes in series representing the upstream and downstream sections of the VAT.

In the DMST, conservation of linear momentum is applied to each stream-tube in order to determine the axial thrust exerted by the fluid on the portion of the actuator disc bounded by that stream-tube. The axial thrust is then used to calculate the extracted power and subsequently the power coefficient. Since the same governing equations apply to each disc in Figure 2, they are only presented here for one disc; thus the *up* and *down* subscripts included in Figure 2 are omitted, but the numbered subscripts identifying specific regions within the stream-tube are included. From conservation of linear momentum, the axial thrust, T, exerted by the disc on

the fluid can be calculated as:

$$T = V_1(\rho AV)_1 - V_4(\rho AV)_4 \tag{1}$$

where A is the cross-sectional area of the disc and V is the fluid velocity. From continuity, the mass flow rate ($\dot{m} = \rho AV$) through the stream-tube is constant giving:

$$T = \dot{m}(V_1 - V_4) \tag{2}$$

The thrust exerted by the fluid on the disc (which is equal in magnitude but opposite in direction to (2)) can be obtained by applying force equilibrium across the disc to give:

$$T = A_2\,(p_2 - p_3) \tag{3}$$

Energy is conserved between the upstream stations (1 and 2) and between the downstream stations (3 and 4). Applying energy conservation between the upstream and downstream stations of a disc yields:

$$p_1 + \frac{1}{2}\rho {V_1}^2 = p_2 + \frac{1}{2}\rho {V_2}^2 \tag{4}$$

$$p_3 + \frac{1}{2}\rho {V_3}^2 = p_4 + \frac{1}{2}\rho {V_4}^2 \tag{5}$$

It is assumed that stations 1 and 4 are sufficiently far upstream and downstream of the disc, respectively, that the pressures are equal ($p_1 = p_4$) and also that stations 2 and 3 are located immediately upstream and downstream of the disc such that $V_2 = V_3$. Solving for $(p_2 - p_3)$ using Equations (3) and (4) and substituting into Equation (5) gives:

$$T = \frac{1}{2}\rho A_2\left({V_1}^2 - {V_4}^2\right) \tag{6}$$

Equating the thrusts from Equations (2) and (6) and recognising $\dot{m} = \rho A_2 V_2$ gives:

$$V_2 = \frac{V_1 + V_4}{2} \tag{7}$$

The fluid velocity through the disc is, therefore, the average of the upstream and downstream velocities. The axial induction factor, a, quantifies by how much a turbine rotor reduces the upstream flow velocity; it is the fractional reduction in velocity between the free-stream and the disc, and is described mathematically as:

$$a = \frac{V_1 - V_2}{V_1} \tag{8}$$

The local velocity at the disc, V_2 and the downstream velocity, V_4, can now be expressed as a function of the free-stream velocity and the induction factor as:

$$V_2 = V_1 (1 - a) \tag{9}$$

$$V_4 = V_1 (1 - 2a) \tag{10}$$

Substituting Equation (10) into Equation (6), the axial thrust can be defined in terms of the axial induction factor as:

$$T = 2\rho A_2 {V_1}^2 a(1 - a) \tag{11}$$

The stream-wise force coefficient, $C_{\mathrm{x,MOM}}$ (MOM indicates it is calculated from momentum (actuator disc) theory), is defined as the ratio of the thrust to the dynamic pressure,

$$C_{x,MOM} = \frac{2\rho A_2 {V_1}^2 a(1 - a)}{0.5\rho A_2 {V_1}^2} = 4a(1 - a) \tag{12}$$

The power performance coefficient, C_{P}, is the ratio of extracted power (TV_2) to available power:

$$C_{\mathrm{P}} = \frac{TV_2}{0.5\rho A_2 {V_1}^3} = 4a(1 - a)^2 \tag{13}$$

It can be shown that the theoretical maximum C_{P} of a turbine, known as the Betz limit, is 0.59 and is achieved when a =1/3.

2.2. Important Model Assumptions

Some important fundamental assumptions of the BEMT model are now presented to provide context for the model theory presented in subsequent sections:

1. Pressure recovery between tandem actuator discs. DMST models assume that there is sufficient slowing of the flow for pressure to recover to the ambient value between the actuator discs within the turbine rotor. This is necessary in order to calculate a recovered flow velocity, which can be used for the downstream calculation. However, in the peripheral regions of the turbine, there is limited space between the disc and this assumption leads to over prediction of the recovered flow speeds in these regions.

2. Flow expansion only occurs in the horizontal (x-y) plane. Although flow is likely to expand in both the horizontal and vertical directions in response to slowing of the fluid speed, flow expansion is limited to the horizontal plane. The consequence of omitting flow expansion in the vertical plane is a small overestimation in the hydrodynamic performance of a VAT [37].

3. Induction only occurs in the stream-wise direction (i.e. tangential induction is neglected). Blade element theory (BET) methods for HATs allow calculation of a tangential induction factor that quantifies wake rotation [38]. This induced flow perpendicular to stream-wise induction conserves angular momentum as a reaction to the flow rotating the blades. VATs also experience similar conditions, although the wake is deflected rather than rotated. Ferreira's BEMT model [37] shows that neglecting tangential induction results in an underestimation of the tangential force coefficient downstream and an overestimation of the tangential force

coefficient for small regions of the upstream. As the tangential forces for the majority of the upstream are unaffected by tangential induction, this research adopts the common practice amongst researchers of resolving induction in only the stream-wise direction.

4. Straight stream-tubes: Where stream-tube expansion is accounted for, it is assumed that the stream-tubes are straight (see Figure 8) as per Sharpe's method, rather than sudden expansion at the mid-plan.

2.3. Blade Element Theory

The fluid dynamics of VATs are significantly more complicated than their horizontal axis counterparts. The variation in azimuthal position (θ) of the blade (see Figure 3) as it rotates through 360° results in variations in relative velocity (V_{rel}), angle of attack (α), lift force (F_{L}) and drag force (F_{D}).

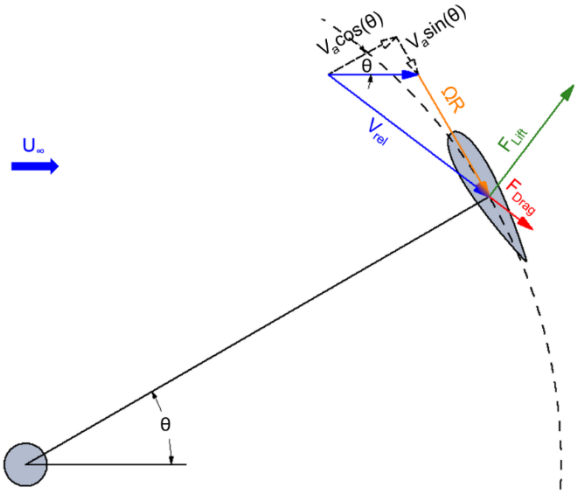

Figure 3: Schematic showing angles, forces and velocities on the blade element.

The relative velocity and the angle of attack are determined using:

$$V_{rel} = \sqrt{(V_a\, cos(\theta))^2 + (V_a\, sin(\theta) + \Omega R)^2} \tag{14}$$

$$\alpha = tan^{-1}\left(\frac{V_a\, cos(\theta)}{V_a\, sin(\theta) + \Omega R}\right) \tag{15}$$

where V_a is the induced actuator velocity, as defined in Equation (9), R is the turbine radius and Ω is the turbine angular rotational velocity.

The lift and drag forces generated by the fluid on a blade element can also be expressed as forces tangential and normal to the direction of travel (Figure 4).The non-dimensionalised tangential and normal force coefficients can, therefore, be determined using the tangential and normal components of the lift and drag coefficients as defined in Equation (16).

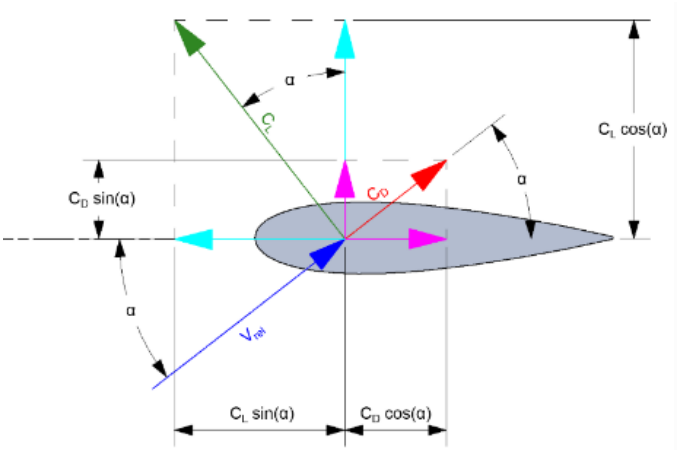

Figure 4: Schematic showing how lift and drag are related to the chord tangential and normal coefficients.

$$C_{\mathrm{T}} = C_{\mathrm{L}} \sin(\alpha) - C_{\mathrm{D}} \cos(\alpha)$$
$$C_{\mathrm{N}} = C_{\mathrm{L}} \cos(\alpha) + C_{\mathrm{D}} \sin(\alpha) \tag{16}$$

The tangential and normal forces are then determined from the tangential and normal coefficients as:

$$F_{\mathrm{T}} = \frac{1}{2} C_{\mathrm{T}} \rho \, A_c {V_{rel}}^2$$
$$F_{\mathrm{N}} = \frac{1}{2} C_{\mathrm{N}} \rho \, A_c {V_{rel}}^2 \tag{17}$$

A schematic of one of the multiple stream-tubes of the DMST is shown in Figure 5 where $\Delta\theta$ is the angular portion of the azimuthal position spanned by the stream-tube. As already mentioned, it is assumed that pressure recovers to free-stream level between the upstream and downstream discs and so the incoming, or recovered, flow for the downstream is denoted V_{rec}. The stream-tubecross-sectional area is defined as:

$$A_s = \Delta L_{\mathrm{B}} R \Delta\theta \cos\theta \tag{18}$$

where ΔL_{B}, is the vertical height of the stream-tube section.

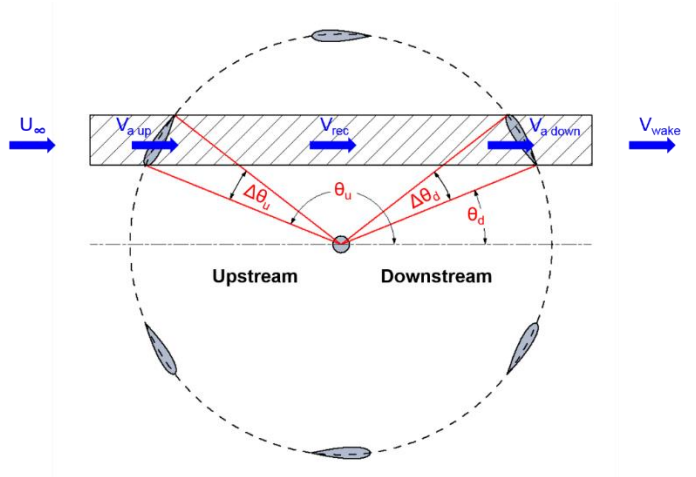

Figure 5: Definition of stream tube geometry (Note. Tube width is not necessarily equal to chord-length).

Each of the N_B blade elements will spend $\frac{\Delta\theta}{2\pi}$ of the time in a particular stream-tube; therefore, the axial thrust for a particular stream-tube can be related to the stream-wise force F_x exerted on an individual blade element as it passes through the stream-tube as follows:

$$T = N_B F_x \frac{\Delta\theta}{2\pi} \tag{19}$$

Substituting for T from Equation (11) and combining with Equation (18) yields:

$$\frac{N_B F_x}{8\pi\rho R\Delta L_B cos(\theta) {U_\infty}^2} = a(1-a) \tag{20}$$

The tangential and normal forces on a blade element and the stream-wise resultant, F_x, are shown in Figure 6 where it can be seen that the resultant $F_x$is given by:

$$F_x = (F_N \cos(\theta) - F_T \sin(\theta)) \tag{21}$$

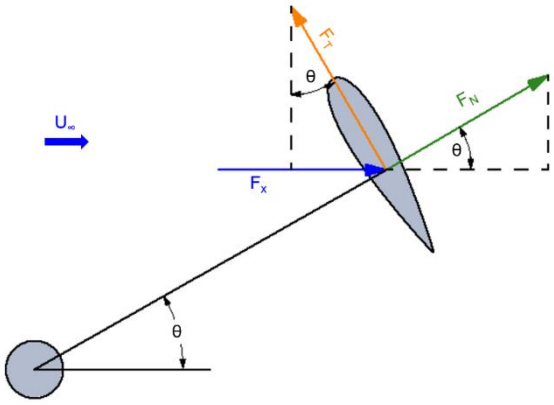

Figure 6: Schematic of normal, tangential and stream-wise forces acting on a blade element.

Combining Equations (16), (17), (20), and (21), the force coefficient for the BET model $C_{x,BET}$ becomes:

$$C_{x,BET} = \frac{N_B c}{8\pi R}\left(\frac{V_{rel}}{U_\infty}\right)^2 \sec(\theta)(C_N \cos(\theta) - C_T \sin(\theta)) \quad (22)$$

2.4. Graphical Method for Determining Induction Factors

To determine the axial induction factor for a stream-tube, which then enables calculation of induced velocities and their resulting forces on blade elements, two different approaches can be used. The first and, by far, the most commonly used involves an iteration process where a is refined according to:

$$a = C_{x,BET} + a^2 \quad (23)$$

This method suffers convergence issues for highly loaded rotors or high solidity rotors and so the graphical approach first introduced by McIntosh *et al.* [22] was implemented in our DMST model. The graphical approach involves generating two functions for the force coefficient, C_x, using $C_{x,MOM}$ and $C_{x,BET}$ (see Figure 7). If the two functions are graphed for different values of a; the point of intersection of the graphs indicates the appropriate value of a. If one only uses Equation (12) (i.e. the momentum model) for the force coefficient, a reversed wake occurs for $a > 0.5$; this is erroneous and is due to the fact that for these values of a the majority of the fluid passes around the rotor, rather than through it, meaning the assumption that all of the flow passes through the enclosing stream-tube no longer holds true. The following empirical correction for the momentum model for high induction factors ($a > 0.4$) was developed by Glauert [13]:

$$C_x(a > 0.4) = 0.86 + 1.56(a - 0.143)^2 \quad (24)$$

To determine $C_{x,MOM}$ then, Equation (12) is used for $a \leq 0.4$ and Equation (24) is used for $a > 0.4$. To determine $C_{x,BET}$, Equation (22) alone is used.

The graphical approach for determining the axial induction factor is now described. $C_{x,MOM}$ is calculated at the outset of the BEMT computation (twice in total upstream and downstream) while $C_{x,BET}$ is calculated for each individual stream-tube. The a value is seeded in the range of -1 to +1 (as recommended by McIntosh *et al.* [22]) in increments of 0.001. For each seeded value of a, the sign of ($C_{x,BET} - C_{x,MOM}$) is calculated and compared to that for the previous value of a so as to determine any crossing of the two force coefficient functions. If a crossing has occurred, then the current value of a is saved as a possible candidate value and the model then proceeds to the next seeded a value until all possible candidate values have been identified. In most cases, there will be only one crossing and the corresponding candidate value of a is selected as the induction factor; this is shown in Figure 7 (a) where there is a unique solution at $a = 0.275$.

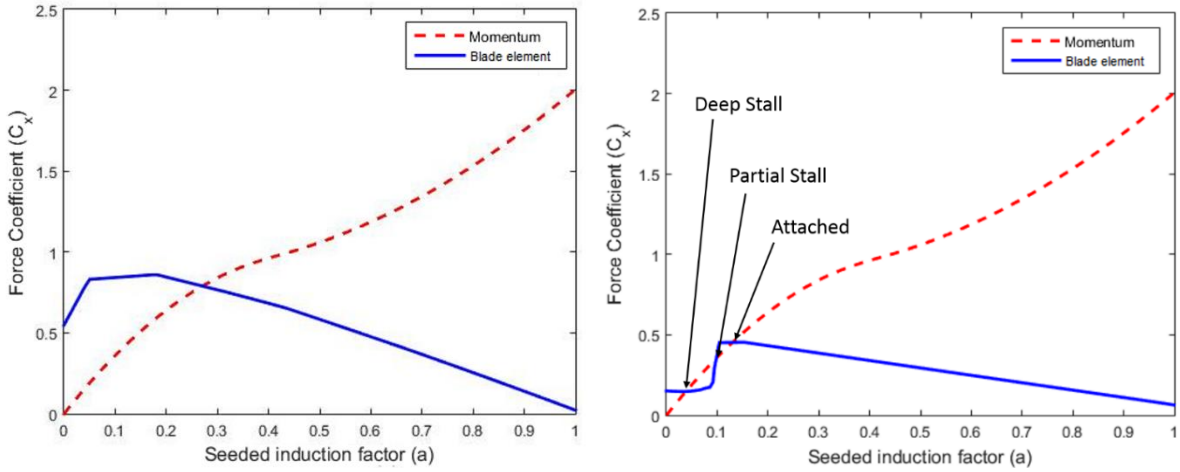

(a) (b)

Figure 7: Graphs of $C_{x,MOM}$ and $C_{x,BET}$ for: (a) a single crossing point and (b) a triple crossing point.

There are conditions, however, that result in multiple crossing points (Figure 7 (b)). This usually happens for highly loaded rotors and/or high solidity devices. The onset of blade stall results in a sharp drop in force coefficient resulting in multiple crossing points. McIntosh *et al.*[22] explain in detail the advantage of the graphical scheme over the iterative approach in this regard as it identifies all crossing points and allows the correct value of, a, to be selected. This is based on the current flow state, whereas, the iterative approach fails to determine any solution. Multiple crossing points are a consequence of blade stall and can occur during the onset of stall or flow reattachment; it is this issue that leads to convergence problems in the iterative scheme particularly for highly loaded rotors [22]. Each of the three crossing points in Figure 7 (b) defines a different flow state: (1) attached, (2) partial stall and (3) deep stall; however, partial stall is unstable and should never emerge as a solution [22]. Knowledge of the previous stream-tube solution is used to identify the most suitable of the attached or deep stall solutions.

For each stream-tube, once the appropriate values of a are known the induced velocities (both upstream and downstream) are recalculated, as are the relative velocities and angles of attack. The Reynolds numbers are recalculated to determine the appropriate lift and drag coefficients from a prescribed database [32]. Subsequently, forces and overall coefficients are calculated.

2.5. Corrections to Basic BEMT Model

Various corrections for the basic BEMT model have been developed by other researchers in an effort to correct or improve model accuracy. Corrections to account for flow expansion, finite aspect ratio blades and dynamic stall and variation of fluid velocity through the turbine height can all be incorporated into the developed model and their effects on model performance assessed. The corrections are implemented via function files in MATLAB which allows the corrections to be included or excluded from a model simulation.

2.5.1. Flow Expansion

The difficulty in accounting for flow expansion in a BEMT model is the delineation of the

boundaries of the individual stream-tubes since the azimuthal positions of the boundaries depend on the amount of flow expansion and, therefore, also on the induction factors. The method proposed by Sharpe and documented by Freris [39] overcomes this difficulty by using a straight stream-tube approximation and calculating each stream-tube induction factor in a specific order (see Figure 8 (a)). Induction factors for the central stream-tube are determined first. This allows calculation of the velocities which in turn allows determination of the degree of expansion of the first stream-tube. The alternate numbering convention shown in Figure 8 (a) means the locations of the boundaries for stream-tubes 2 and 3 will now become known. Induction factors and velocities for stream-tubes 2 and 3 may then be calculated allowing determination of the boundaries for stream-tubes 4 and 5. This process continues until induction factors and velocities for all stream-tubes have been determined.

The objective of a BEMT model is to balance blade element forces with the thrust in the direction of the stream-tube. A consequence of flow expansion is that the direction of the incoming flow changes in a manner that tends to point away from the central stream-tube. For calculation of stream-tube and blade element parameters, a new angle, β, is defined as the angle between the azimuthal position at a stream-tube boundary and the straight stream-tube; this is shown in Figure 8 (b).

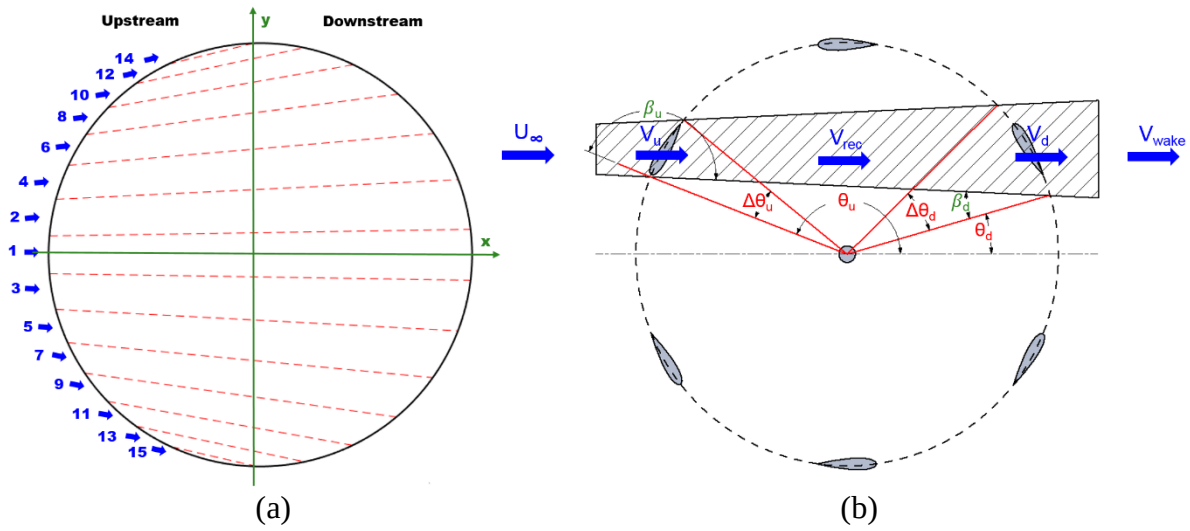

Figure 8:(a) Alternating numbering convention used for determining stream-tube expansion, and (b) flow and angles upstream and downstream of an expanding stream-tube (note. not an accurate representation of expansion, in reality tube would be rotated in an anti-clockwise direction as per (a)).

The normal and tangential forces on a blade element can be transformed into the stream-tube direction using β with $\beta = 0^o$ for the central stream-tube. β is also then used to calculate the upstream and downstream induction factors and the degree of stream-tube expansion for that stream-tube. To demonstrate how to calculate the upstream and downstream actuator surface areas we use the stream-tube shown in Figure 9 with local flow velocities and actuator surface areas labelled. The upstream induction factor, a_u, must be determined before calculating the downstream induction factor, a_d. These are calculated using the graphical method discussed previously. Once both induction factors have been calculated for a stream-tube, the flow speeds V_u and V_d can be easily determined. The tube areas, A_u and A_d, are the areas of the stream-tube cross-section perpendicular to V_u and V_d as shown in Figure 9.

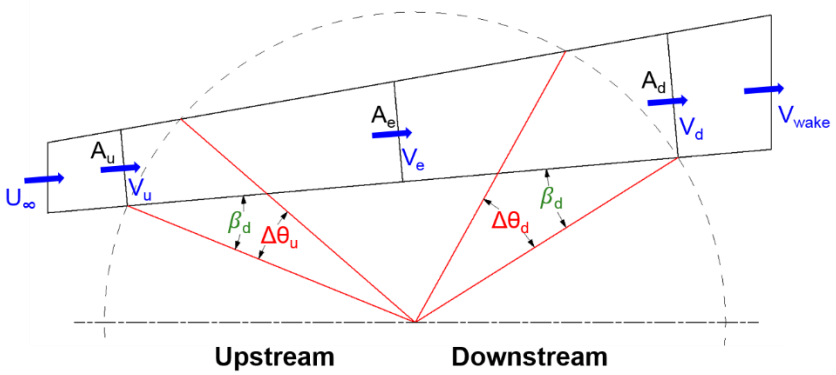

Figure 9: Graphical representation of the relationship between velocities and cross-sectional area due to mass conservation within a stream-tube.

Based on the straight stream-tube assumption, when expansion occurs there is one location between the upstream and downstream actuator surfaces that maintains the original area of the stream-tube prior to expansion. This location is referred to as the equilibrium point and the stream-tube area and flow speed at this point are known as the equilibrium stream-tube area, A_e, and the equilibrium flow speed, V_e(see Figure 9). A_e is the average of the up- and downstream areas:

$$2A_e = A_u + A_d \tag{25}$$

As the stream-tubes are assumed to be enclosed and the fluid density does not vary, conservation of mass gives:

$$V_u A_u = V_e A_e = V_d A_d \tag{26}$$

Combining Equations (25) and (26) gives:

$$2A_e = \frac{A_e V_e}{V_u} + \frac{A_e V_e}{V_d} \tag{27}$$

and simplifying this gives,

$$V_e = \frac{2V_u V_d}{V_u + V_d} \tag{28}$$

V_e should not be confused with V_{rec} which is the flow speed between the tandem actuator surfaces where pressure has recovered. A_e is independent of the induction factors because the straight streamlines pivot about this point for different induction factors. A_e is expressed as:

$$A_e = R|cos(\beta_d)|\Delta\theta\ \Delta L_B \tag{29}$$

where $\Delta\theta = \frac{2\pi}{N_{tubes}}$.

Splitting up the blade length into incremental lengths of ΔL_{B} is required when blades are not straight, such as in the case of a Darrieus VAT, or when a depth-varying velocity profile is added to the model. Conservation of mass allows the up and downstream stream-tube areas, A_u and A_d respectively, to be determined. As mentioned already, the flow expansion of the central stream-tube is determined first before considering the adjacent outer stream-tubes. Therefore, the series of arcs subtended by actuator surfaces is built up cumulatively as the procedure progresses from the centre stream-tube outwards. From Figure 9, it is clear that the boundaries of the adjacent stream-tubes can be determined if the upstream and downstream expansion angles, $\Delta\theta_u$ and $\Delta\theta_d$, are known.

Since A_u can be defined in two ways as:

$$A_u = R|cos(\beta_d)|\Delta\theta_u \, \Delta L_{\mathrm{B}} = \frac{2V_d}{V_u + V_d} R|cos(\beta_d)| \, \Delta L_{\mathrm{B}} \tag{30}$$

we can cancel the common terms to give the upstream expansion angle:

$$\Delta\theta_u = \frac{2V_d}{V_u + V_d} \tag{31}$$

Similarly, we can calculate the downstream expansion angle as:

$$\Delta\theta_d = \frac{2V_u}{V_u + V_d} \tag{32}$$

2.5.2. Finite Aspect Ratio

For an aero/hydrofoil, the aspect ratio (AR) is the ratio of the foil length to the chord-length:

$$AR = \frac{L_{\mathrm{B}}}{c} \tag{33}$$

Foil databases, such as those from Sheldal and Klimas [32], are only available for infinite aspect ratios. Since rotor blades have a finite aspect ratio, the use of an infinite aspect ratio database in a BEMT model can lead to inaccuracies. Corrected C_{L} and C_{D} values can be calculated for foils of finite aspect ratios. Different correction methods are used depending on the values of α and the static stall angle, α_{ss}. As shown in Figure 10, infinite aspect ratio C_{L} values will be larger than those for finite foils at all angles of attack, while infinite aspect ratio C_{D} values will be smaller for $\alpha<\alpha_{ss}$ and larger for $\alpha>\alpha_{ss}$. .

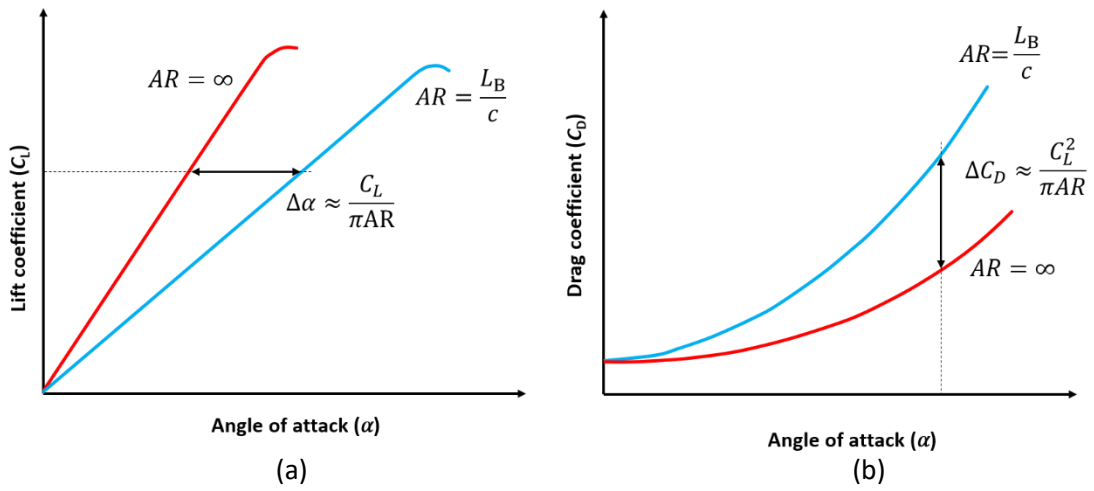

Figure 10: Effect of finite aspect ratio on (a) lift and (b) drag of an aerofoil showing effective angle of attack increase and induced drag increase. (Adapted from White [40])

For angles of attack below α_{ss}, the Lanchester-Prandtl theory can be used to accurately estimate lift and drag characteristics for finite aspect ratio foils from infinite aspect ratio data [33]. Finite aspect ratio blades experience blade tip vortices which cause a downwash and alter the effective angle of attack and aerofoil characteristics. The linear part of the lift curve is calculated using:

$$C_{\mathrm{L}} \approx \frac{2\pi\left(\alpha + 2\frac{h}{c}\right)}{1 + \frac{2}{AR}} \tag{34}$$

where h/c is the maximum camber expressed as a fraction of the chord-length. For aerofoils that are not cambered, h/c is equal to zero. As shown in Figure 10, the effective angle of attack increases and the amount by which it changes can be related to the lift coefficient using the expression:

$$\Delta\alpha \approx \frac{C_{\mathrm{L}}}{\pi AR} \tag{35}$$

The drag coefficient also increases and this increase can be calculated using:

$$\Delta C_{\mathrm{D}} \approx \frac{C_{\mathrm{L}}^2}{\pi AR} \tag{36}$$

For angles of attack greater than the static stall angle and up to 90^{o}, Viterna and Corrigan [34] developed the following set of correction equations:

$$C_{\mathrm{L}_{VC}} = A_1 \sin(2\alpha) + A_2 \frac{\cos^2(\alpha)}{\sin(\alpha)} \tag{37}$$

$$C_{\mathrm{D}_{VC}} = B_1 \sin^2(\alpha) + B_2 \cos(\alpha) \tag{38}$$

where $C_{\mathrm{L}_{VC}}$ and $C_{\mathrm{D}_{VC}}$ are the Viterna and Corrigan corrected lift and drag coefficients,

respectively.

For $AR \leq 50$, the coefficients A_1 and B_1 can be calculated as follows:

$$A_1 = \frac{C_{\mathrm{D}_{max}}}{2} \tag{39}$$

$$B_1 = C_{\mathrm{D}_{max}} \tag{40}$$

where $C_{\mathrm{D}_{max}}$, the maximum drag coefficient for a finite aspect ratio foil, is calculated from the AR value as:

$$\mathrm{C_{D_{max}}} = 1.11 + 0.18\ \mathrm{AR} \tag{41}$$

The variables A_2 and B_2 in equations (39) and (40) are solved at the static stall angle condition for continuity with the 'below stall' data determined using the Lanchester-Prandtl theory.

$$A_2 = \left(C_{\mathrm{L}_{SS}} - C_{\mathrm{D}_{max}} sin(\alpha_{SS})\, cos(\alpha_{SS})\right) \frac{\sin(\alpha_{SS})}{\cos^2(\alpha_{SS})} \tag{42}$$

$$B_2 = C_{\mathrm{D}_{SS}} - \frac{C_{\mathrm{D}_{max}} \sin^2(\alpha_{SS})}{cos(\alpha_{SS})} \tag{43}$$

Castelli *et al.* [35] reported that the data correction method of Viterna and Corrigan resulted in an overestimation of the lift coefficient after the stall angle. Together with a decrease of the drag coefficient, this can result in an overestimation of rotor performance. To avoid this over-prediction, Castelli *et al.* [35] recommended computing modified finite aspect ratio aerofoil characteristics based on a linear interpolation between the infinite aspect ratio values of lift and drag coefficients and the finite aspect ratio coefficients obtained by the Viterna and Corrigan model giving:

$$C_{\mathrm{L}} = \frac{\left(C_{\mathrm{L}_{AR=\infty}} + C_{\mathrm{L}_{VC}}\right)}{2} \tag{44}$$

$$C_{\mathrm{D}} = \frac{\left(C_{\mathrm{D}_{AR=\infty}} + C_{\mathrm{D}_{VC}}\right)}{2} \tag{45}$$

This is the approach that has been adopted in the present BEMT model.

2.5.3. Dynamic Stall

A dynamic stall model was implemented in the BEMT model in order to correct for the use of static foil lift and drag coefficients. Dynamic stall is most significant at lower λ values where the local angle of attack is above the static stall angle. As the blade rotates, the angle of attack changes and a vortex is shed from the leading edge of the foil. Dynamic stall is dependent on a wide range of parameters including foil shape, Mach number, Reynolds number and the rate

of change of angle of attack. The dynamic stall model implemented here is based on Gormont's model [26] for the performance of helicopter rotors, with modifications by Massé [27] and Berg [28] to enable its application to VATs. In order to apply the Gormont model, the time derivative of α ($\dot{\alpha}$) is required.

The Gormont model empirically mimics the hysteresis behaviour of an aerofoil by defining a reference angle of attack at which the static two-dimensional coefficient data is considered. This reference angle of attack, α_{ref}, is expressed as:

$$\alpha_{ref} = \alpha - K_1 \Delta\alpha \tag{46}$$

where,

$$K_1 = \begin{cases} 1 & \text{when } \dot{\alpha} \geq 0 \\ -0.5 & \text{when } \dot{\alpha} < 0 \end{cases} \tag{47}$$

and,

$$\Delta\alpha = \begin{cases} \gamma_1 S & \text{when } S \leq S_c \\ \gamma_1 S_c + \gamma_2 (S - S_c) & \text{when } S > S_c \end{cases} \tag{48}$$

The variables in Equation (48) have the following expressions:

$$\gamma_1 = \begin{cases} \frac{\gamma_2}{2} & \text{for lift} \\ 0 & \text{for drag} \end{cases} \tag{49}$$

$$\gamma_2 = \gamma_{max} max\left\{0, \min\left[\frac{1, M_a - M_2}{M_2 - M_1}\right]\right\} \tag{50}$$

$$S_c = 0.06 + 1.5(0.06 - t_c) \tag{51}$$

where t_c is the thickness of the aero/hydrofoil.

$$S = \sqrt{\frac{c\dot{\alpha}}{2V_{rel}}} \tag{52}$$

In Equation (50), M_a is the Mach number and is given by:

$$M_a = \left|\frac{V_{rel}}{c_{speed}}\right| \tag{53}$$

Expressions for the other variables in Equation (50) are given in Table 1.

Table 1: Specific forms of M_1, M_2, and γ_{max} for lift and drag.

	Lift	Drag
M_1	$0.4 + 5(0.06 - t_c)$	0.2
M_2	$0.9 + 2.5(0.06 - t_c)$	$0.7 + 2.5(0.06 - t_c)$
γ_{max}	$1.4 - 6(0.06 - t_c)$	$1.0 - 2.5(0.06 - t_c)$

The dynamic stall lift and drag coefficients are then calculated as:

$$C_{\mathrm{L}}^{dyn} = C_{\mathrm{L}}(\alpha_0) + m(\alpha - \alpha_0) \tag{54}$$

$$C_{\mathrm{D}}^{dyn} = C_{\mathrm{D}}(\alpha_{ref}) \tag{55}$$

where α_0 is any convenient angle of attack but is typically taken as the zero-lift angle of attack and m is calculated as:

$$m = \left[\frac{C_{\mathrm{L}}(\alpha_{ref}) - C_{\mathrm{L}}(\alpha_0)}{\alpha_{ref} - \alpha_0}, \frac{C_{\mathrm{L}}(\alpha_{SS}) - C_{\mathrm{L}}(\alpha_0)}{\alpha_{SS} - \alpha_0}\right] \tag{56}$$

In Gormont's model for helicopter blades the maximum angle of attack reached is much lower than in the case of a VAT blade. As observed by Massé [17] and reported by Masson *et al.* [41], this means that the Gormont model over predicts the effects of the dynamic stall on VAT performances. In order to avoid this, Massé [27] proposed to calculate modified dynamic coefficients based on a linear interpolation between the dynamic coefficients predicted by the Gormont model and the static coefficients as follows:

$$C_{\mathrm{L}}^{mod} = \begin{cases} C_{\mathrm{L}} + \left[\dfrac{A_{\mathrm{M}}\alpha_{ss} - \alpha}{A_{\mathrm{M}}\alpha_{ss} - \alpha_{ss}}\right]\left(C_{\mathrm{L}}^{dyn} - C_{\mathrm{L}}\right) & \alpha \le A_{\mathrm{M}}\alpha_{ss} \\ C_{\mathrm{L}} & \alpha > A_{\mathrm{M}}\alpha_{ss} \end{cases} \tag{57}$$

$$C_{\mathrm{D}}^{mod} = \begin{cases} C_{\mathrm{D}} + \left[\dfrac{A_{\mathrm{M}}\alpha_{ss} - \alpha}{A_{\mathrm{M}}\alpha_{ss} - \alpha_{ss}}\right]\left(C_{\mathrm{D}}^{dyn} - C_{\mathrm{D}}\right) & \alpha \le A_{\mathrm{M}}\alpha_{ss} \\ C_{\mathrm{D}} & \alpha > A_{\mathrm{M}}\alpha_{ss} \end{cases} \tag{58}$$

where $A_M = 6$ is a revised value for A_M proposed by Berg [28] to replace the initial value of $A_M = 1.8$ proposed by Massé; Berg found the revised value gave better agreement with experimental data for a SANDIA wind turbine. Berg [28] also recommended that α_{ss} be taken as the angle where C_{L} is no longer increasing linearly as opposed to previous work which took α_{ss} as the angle of maximum C_{L}. These dynamic stall corrections were incorporated into the model.

2.5.4. Strut Effects

The aerodynamic behaviour of struts affects the torque of a turbine and may be accounted for in BEMT models through the use of three corrections: (1) the equivalent tangential force, (2)

drag due to the strut arm and (3) additional drag due to the junction between the strut arm and the blade. The junction of the strut and blade also increases the effective turbine solidity locally at the tips of the blades and is a source of vortex generation in the tip area. The following corrections based on those of Kirke and Paillard [48] were implemented in the BEMT model.

Firstly, the equivalent tangential force is obtained by the integration of the tangential force along the blades, the formulation of which has already been described. The power loss associated with the strut drag is determined using Equation (59) which relates the drag due to the struts and rotational velocity of the rotor to power:

$$\Delta P_{Strut} = \frac{1}{2} N_{Strut}\, \rho \left(\frac{c}{\cos(\psi)} \right) C_{d_{Strut}} \Omega^3 \frac{R^4}{4} \tag{59}$$

where, N_{Strut} is the total number of struts on the rotor. $C_{d_{Strut}}$ is the drag coefficient of the strut at the specified Reynolds number. ψ is the angle of the struts relative to the horizontal plane.

The additional junction drag is obtained by the use of the following thickness drag coefficient after Hoerner [49]:

$$\Delta D_{Junction} = C_{d_{Junction}} q t^2 \tag{60}$$

where,

$$C_{d_{Junction}} = 17 \left(\frac{t}{c} \right)^2 - 0.05 \tag{61}$$

and the dynamic pressure, q, is defined as

$$q = \frac{1}{2} \rho {V_{rel}}^2 \tag{62}$$

Finally, the change in power due to the added junction drag is determined by:

$$\Delta P_{Junction} = N_{Strut} \Delta D_{Junction}\, \Omega R \tag{63}$$

As the works of Mannion et al. [12] and Kirke and Paillard [48] showed that strut effects can have a significant effect on turbine rotor performance, it was deemed necessary to account for these effects in the development of the current model presented here.

2.5.5. Velocity profile

The BEMT model has the capability to account for the vertical variation in velocity distribution through a fluid. The model allows for incremental calculations along the vertical length of the blade, therefore allowing the incoming velocity to be varied along the vertical span of the turbine rotor. The water velocity profile is described using a power law where the velocity at height, z, above the seabed (U_z) is defined as:

$$U_z = \left(\frac{z}{\zeta h_w}\right)^{\frac{1}{n}} \overline{U} \tag{64}$$

where ζ is the roughness coefficient, h_w is the total water depth and $\overline{U}$ is the depth averaged velocity. Values of n = 7 and ζ = 0.4 are used as recommended by literature [42]. It has been shown that on average the power law accurately represented the velocity profile for numerous sites for over one month's worth of ADCP data [42].

Although developed for tidal turbines, the BEMT model is also applicable to wind turbines and one of the performance assessment applications in the results section is a 500 kW wind turbine. For large turbines like this, it is important to account for the variation of wind velocity with height. The following formula from McIntosh [43] is used to estimate the wind shear velocity profile:

$$U_z = U_{ref} \frac{\left(ln\frac{z}{z_0}\right)}{\left(ln\frac{z_{ref}}{z_0}\right)} \tag{65}$$

U_{ref} is the wind velocity at a reference height, z_{ref}, while z_0 is the terrain roughness height. McIntosh [43] presents a table of suggested values of z_0 for different surface terrains.

2.6. Model Structure and Solution Procedure

The model was created by encoding the relevant actuator disc and blade element model equations and the graphical approach for determination of induction factor within MATLAB. This basic BEMT model was then augmented by encoding corrections to the governing equations for the effects of flow expansion, finite aspect ratio blades, dynamic stall and a depth-varying velocity profile. Code to read in required input data and generate required model output was also written. The final BEMT model is structured in three separate parts as follows:

Stage 1 - *Model Initialisation*: The model is initiated by reading in the required input data including turbine geometry, free-stream flow conditions, lift and drag coefficients for the particular aerofoil, and the specification of the stream-tube geometry.

Stage 2 – *Local Solution*: First, fluid velocities are calculated using seeded induction factor values. These velocities are subsequently used to calculate more accurate induction factor values using the graphical approach and the velocities are then recalculated. This procedure is repeated for every actuator point (2 per stream-tube, i.e. upstream and downstream) around the turbine swept area. At the end of the stage, all local flow velocities, angles and dynamic forces for each stream-tube are stored for a particular λ value. Corrective methods can be switched on and off in the model in an attempt to improve the model accuracy.

Stage 3 – *Global Solution*: the contributions from each stream-tube are calculated and combined to determine the performance of the rotor as a whole in terms of torque, thrust and power. The relevant model variables are output for interrogation/analysis.

2.7. Model Geometry and Foil Characteristic Data

This section outlines how the turbine rotor perimeter is subdivided into a collection of actuator surfaces and discusses the characteristic aerofoil data for lift and drag that are incorporated into the model.

2.7.1. Rotor Mesh and Stream-tube Expansion

The perimeter of the turbine rotor is subdivided into a number of sections which make up the actuator discs. As DMST models use two actuator discs in tandem, the 15 tubes shown in Figure 11(a) have a total of 30 actuator surfaces (15 upstream and 15 downstream). The inclusion of flow expansion adds more complexity to the model since upstream stream-tube areas will be smaller than the downstream areas (Figure 11 (b)). The increasing cross-sectional area of each stream-tube in the stream-wise direction means that the rotor spends more time in the downstream section of each stream-tube compared to the upstream section. The symmetrical nature of the stream-tube expansion shown in Figure 11 (b) is a consequence of neglecting tangential induction.

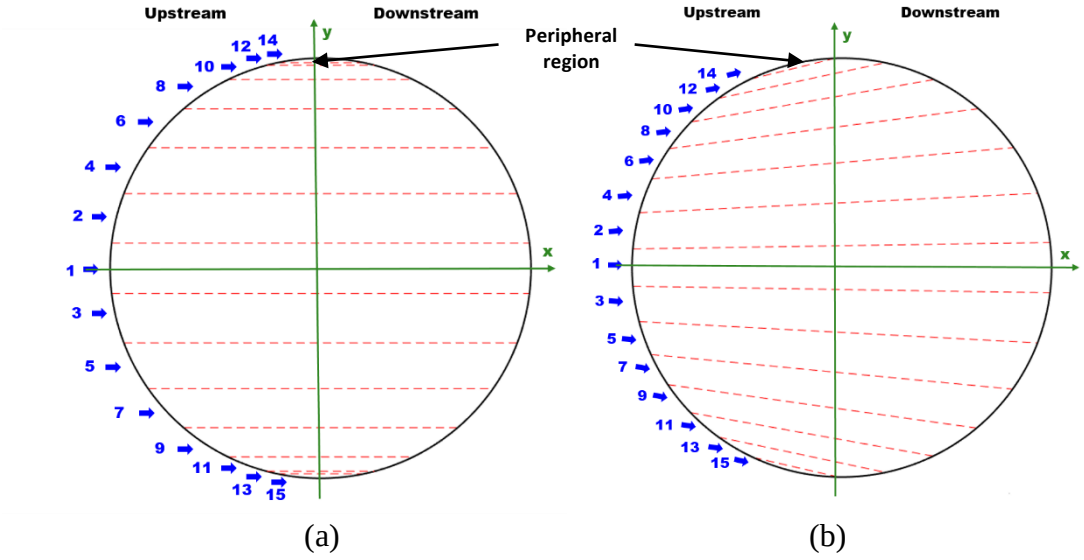

Figure 11: Example of stream-tube division (a) without flow expansion and (b) with flow expansion.

2.7.2. Aerofoil Lift and Drag Data

The performance of any turbine rotor is greatly influenced by the choice of aero/hydrofoils and foil lift and drag data is, therefore, a required input to all BEMT models to enable calculation of blade element forces. These data are usually stored in lookup tables that contain the coefficients of lift and drag for a range of angles of attack and Reynolds numbers (chord-length). All of the model simulations in this research use symmetric NACA aerofoils and the appropriate aerofoil database sourced from Sheldahl and Klimas [32].

Reynolds number has a significant impact on the aerodynamic/hydrodynamic characteristics of the aerofoil/hydrofoil and Reynolds number varies as the blade rotates. It is, therefore, imperative that a VAT performance estimation model incorporates the correct Reynolds number for every azimuthal position. The developed BEMT model recalculates the Reynolds number at each azimuthal location around the path of rotation and for every value of a, since there is a direct relationship between a, Reynolds number and relative velocity. Figure 12 and Figure 13 show how C_{L} and C_{D} vary for a range of α values and for different Reynolds numbers. The data presented in the figures is for a NACA 0018 aerofoil section from the Sheldahl and Klimas database.

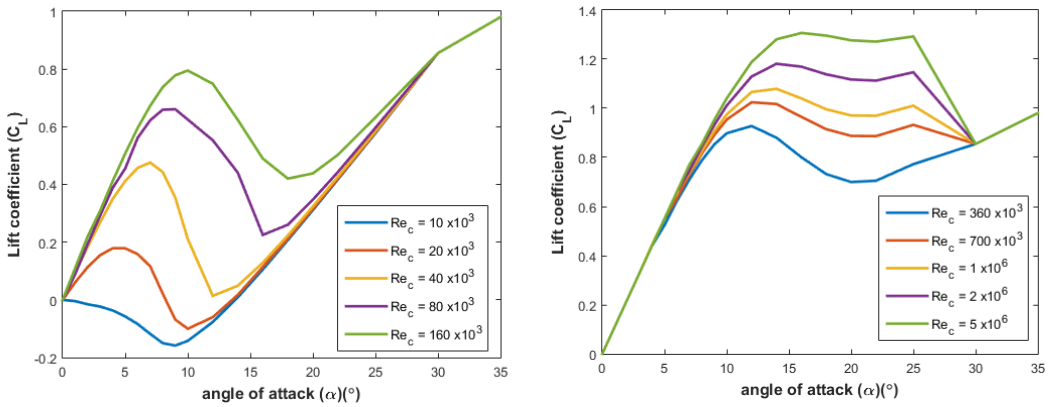

(a) (b)

Figure 12: Variation of lift coefficient with Reynolds number over a range of angles of attack.

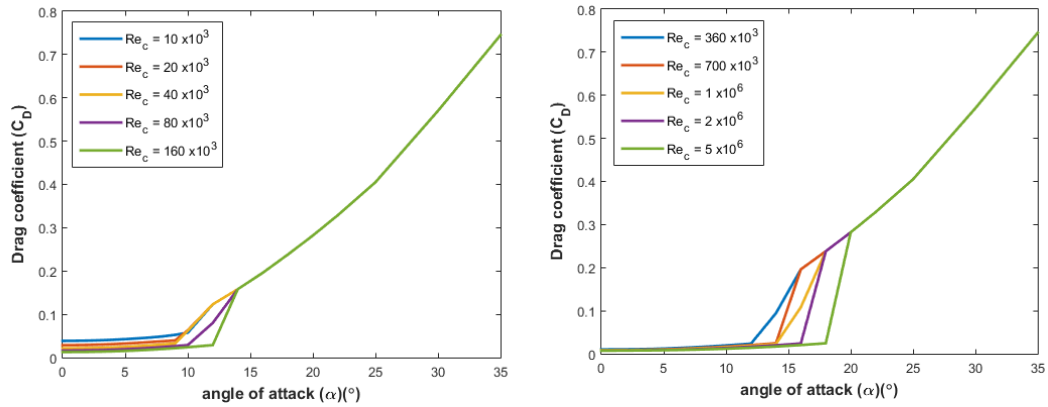

(a) (b)

Figure 13: Variation of drag coefficient with Reynolds number over a range of angles of attack.

Sheldahl and Klimas [32] used the Profile (panel method) code of Eppler and Somers [44], often known simply as Eppler's model, in conjunction with experimental data to produce lift and drag characteristic data for NACA 0012, 0015, 0018, 0021 and 0025 series aerofoil profiles over an extensive range of angles of attack and Reynolds numbers. Pre- and early-stall section information was calculated, using the Profile code. Late- and post-stall section characteristics were taken from the measured data. The high angle of attack data assumes Reynolds number

independence, in that high angle of attack data is the same across all Reynolds numbers. It also assumes independence for the thicker sections (the NACA 0015 data are used for the 0018, 0021 and 0025 sections). These data are frequently used in blade element momentum theory models (this being their intended use) but are sometimes mistakenly referred to as being of purely experimental origin [45]. As the use of the DARTER code conflates static and dynamic stall performance, the "static" coefficients published by Sheldahl and Klimas have received criticism in the literature [46]. Despite these criticisms, its comprehensive nature (it covers a large range of aerofoil sections, angles of attack and Reynolds numbers) means it is still the data set most commonly used in BEMT models.

2.8. Model Outputs

The overall turbine torque can be determined by taking moments about the axis of rotation of the forces acting on a unit length of blade as shown in Figure 14. This torque may then be expressed as:

$$Q = \frac{1}{2} {V_{rel}}^2 \rho c \left(C_T R \pm C_N \frac{c}{4} \right) \tag{66}$$

The thrust, T, is an instantaneous force (in that it occurs only as a blade crosses a stream-tube) but we require a time-averaged force. To obtain this, the chord-length, c, in Equation (66) is replaced by:

$$\tilde{c} = \frac{N c \Delta\theta}{2\pi} \tag{67}$$

where $\frac{\Delta\theta}{2\pi}$ is the probability of a given blade being in any particular position during a particular time interval. From Equation (30), for a unit length of blade $A = R|cos(\beta_d)|\Delta\theta$. Rearranging in terms of $\Delta\theta$ and substituting into Equation (67), therefore, gives:

$$\tilde{c} = \frac{N_\mathrm{B} c \mathrm{A}}{|cos(\beta_d)| 2\pi R} = \frac{N_\mathrm{B} c}{2\pi R} A |sec(\beta_d)| \tag{68}$$

Replacing c in Equation (66) with $\tilde{c}$ gives the following expressions for the upstream (Q_u) and downstream (Q_d) torque:

$$Q_\mathrm{u} = \frac{1}{2} \rho {V_{\mathrm{rel}_\mathrm{u}}}^2 \frac{N_\mathrm{B} c}{2\pi R} |sec(\beta_d)| A_u \left(C_{\mathrm{T}_\mathrm{u}} R + C_{\mathrm{N}_\mathrm{u}} \frac{c}{4} \right) \tag{69}$$

$$Q_\mathrm{d} = \frac{1}{2} \rho {V_{\mathrm{rel}_\mathrm{d}}}^2 \frac{N_\mathrm{B} c}{2\pi R} |sec(\beta_d)| A_d \left(C_{T_d} R - C_{N_d} \frac{c}{4} \right) \tag{70}$$

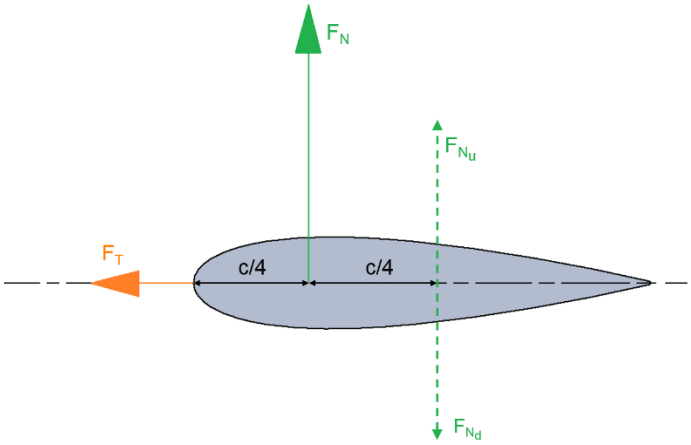

Figure 14: Blade element forces, showing the normal changing direction between up and downstream at the centre of rotation.

The average torque on a whole turbine with blades of length L_B can then be determined by integrating along the span of the blade as well as around the circumference of the rotor and is given by:

$$Q_{avg} = \frac{N_B c}{2\pi R}\rho R \int_0^{L_B}\int_{-\frac{\pi}{2}}^{\frac{\pi}{2}}\left[{V_{rel_u}}^2 V_d\left(C_{T_u}R + C_{N_u}\frac{c}{4}\right) + {V_{rel_d}}^2 V_u\left(C_{T_d}R - C_{N_d}\frac{c}{4}\right)\right]\frac{1}{(V_u + V_d)}\,d\beta dL_B \tag{71}$$

The thrust force on the turbine can be determined by integrating the stream-wise forces:

$$T_{avg} = \frac{N_B c}{2\pi}\rho \int_0^{L_B}\int_{-\frac{\pi}{2}}^{\frac{\pi}{2}}\left[{V_{rel_u}}^2 V_d\left(C_{N_u}\cos(\beta_d) - C_{T_u}\sin(\beta_d)\right) + {V_{rel_d}}^2 V_u\left(C_{N_d}\cos(\beta_d) - C_{T_d}\sin(\beta_d)\right)\right]\frac{1}{(V_u + V_d)}\,d\beta dL_B \tag{72}$$

As mentioned by Sharpe [39], calculation of thrust in this way is not completely accurate, particularly for high λ values, because the expanding streamlines are not parallel and so stream-wise forces cannot be added algebraically. However, it is the most common method used in conjunction with the Sharpe method for flow expansion. The overall turbine power coefficient, C_P, is defined as:

$$C_P = \frac{Q_{avg}\Omega}{0.5\rho A {U_\infty}^3} \tag{73}$$

3. Results

The performance of the BEMT model was assessed first, for a low solidity VAWT and second, for a high solidity VATT (where solidity, σ, is defined as per Equation (69)). In each case, modelled power performance data were compared with measured data obtained from published

literature and the effects of the various corrections on model performance were investigated. The confined nature of the flow for the tidal turbine case study was suspected to affect model performance so the model (including all corrections) was subsequently applied to a high solidity wind turbine in unconfined flow. Finally, the effect of inclusion of a correction for support struts was assessed for all three turbines.

3.1. Low Solidity Wind Turbine and High Solidity Tidal Turbine

The low solidity wind turbine was a full-scale 2-bladed 500 kW VAWT, the VAWT-850, tested by Mays *et al.* [51] while the high solidity tidal turbine was a 3-bladed scale model VATT tested by Bachant and Wosnik [52]. The main physical characteristics of the turbines are summarised in Table 2. Five different models of each turbine were run to assess the effect of the various corrections on model performance both individually and cumulatively. The models are listed in Table 3 along with their respective acronyms. A wind velocity profile was incorporated into the BEMT for the VAWT-850 using Equation (64). As the turbine was deployed in relatively open terrain, a terrain value of z_0 = 0.03 m was used for the velocity profile. As the high solidity turbine was tow tested, the inlet velocity was taken as the tow speed. The power performance results from the various models are presented as C_P versus λ curves.

$$\sigma = \frac{\text{total blade area}}{\text{rotor swept area}} = \frac{N_\mathrm{B} c L_\mathrm{B}}{\pi D L_\mathrm{B}} = \frac{N_\mathrm{B} c}{\pi D} \tag{69}$$

Table 2: Details of the VATs used to assess model accuracy.

Blades $\boldsymbol{N_\mathrm{B}}$	Turbine Type	Diameter $\boldsymbol{D}$ (m)	Chord-length $\boldsymbol{c}$ (m)	Blade Length $\boldsymbol{L_\mathrm{B}}$ (m)	Foil Profile	Solidity $\boldsymbol{\sigma}$
2	Wind	35	1.5 to 1.75	24.3	NACA 0018	0.03
3	Tidal	1	0.14	1	NACA 0021	0.28

Table 3: Description of model acronyms presented in figures.

Description	Model Acronym
Basic BEMT model without any corrections.	Basic-BEMT
Basic BEMT plus flow expansion correction only.	BEMT-FE
Basic BEMT plus finite aspect ratio correction only.	BEMT-FAR
Basic BEMT plus dynamic stall model only.	BEMT-DS

Basic BEMT plus all flow corrections – flow expansion, finite aspect ratio and dynamic stall.	BEMT-ALL

Figure 15 (a) compares BEMT model results with experimental data for the low solidity wind turbine while Table 4 presents the average RMSE in C_P calculated for all of the models. The basic BEMT model predicts the appropriate performance trend with the peak performance (C_{Pmax}) occurring at the same λ value of 3.5 as the measured data but it overpredicts C_P for all λ values. Looking first at the individual effects of the model correction, when flow expansion is included there is no obvious change in model results for $\lambda < 3$ but model accuracy is improved for higher λ values (i.e. $\lambda > 3.5$); this is most likely because the stream-tubes experience greater expansion at higher λ values. The finite aspect ratio correction has a negligible effect overall although it does slightly improve model accuracy at lower λ values ($\lambda < 2$). Including dynamic stall leads to reduction of C_P values for lower λ values ($\lambda < 4$) and thus better agreement with measured data for this portion of the power curve. Of all three corrections, this one results in the most accurate prediction of C_{Pmax} compared to the basic BEMT model with a difference of just 6.4 % compared to the measured value. As λ increases above 4, the effect of the dynamic stall model diminishes and above $\lambda = 5$ it has no discernible effect. This is likely because as λ increases the ranges of α values experienced by the VAT blades reduces until the turbine operates completely out of stall and dynamic stall is no longer significant. Figure 15(b) compares the C_P curve predicted by the BEMT model when all three corrections are applied together with the measured data of Mays *et al.* [51] and the basic BEMT model predictions. It can be seen that model performance is significantly improved when the corrections are included. Although the BEMT-All still over-predicts C_P, the level of over-prediction is much reduced from the Basic BEMT model. The error in C_{Pmax} was reduced from 17.5 % to 6.4 % at C_{Pmax} and the average RMSE for all measured data points was reduced from 0.079 to 0.034.

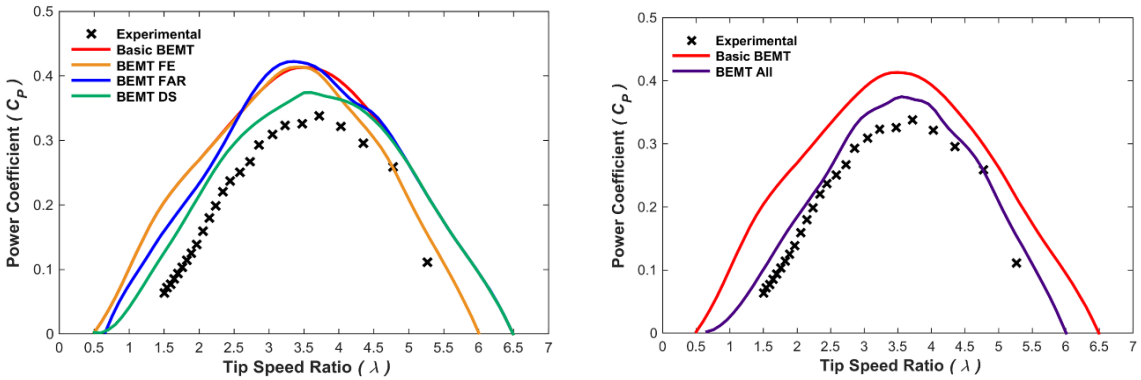

(a) (b)

Figure 15: Comparison of BEMT modelled C_P with measured data [51] for the low solidity VAWT.

Figure 16 (a) presents the comparison of C_P results with measured data for the high solidity tidal turbine rotor [52]. Again RMSEs in C_P are shown in Table 4 for all of the models. In all model cases, it can be seen that the power curve is shifted to the right and C_{Pmax} is over-predicted. The Basic BEMT model over-predicts C_{Pmax} by 46.9 % and determines the optimum λ value to be 2.4 compared to the measured value of 1.9. Looking at the effects of the

corrections individually, flow expansion results in lower C_P values and thus improved accuracy for $\lambda > 2.2$ but has a negligible effect for λ values lower than this, this is similar to the observations for the low solidity rotor. Inclusion of the finite aspect ratio correction has the effect of reducing C_P in the regions where stall dominates ($\lambda < 1.5$), while marginally increasing C_P in the peak performance region. Looking lastly at the effect of the dynamic stall correction, initially, deep stall conditions exist and the effect of dynamic stall is to permit larger C_L which results in higher C_P values than the Basic BEMT. As λ increases towards the optimum value, dynamic stall has the effect of reducing C_P. For tip speed ratios higher than the optimum value, the dynamic stall correction has a negligible effect on the model performance.

Figure 16 (b) compares the BEMT model C_P values when all three corrections are included together with the measured values and the basic BEMT model. While the corrections have little effect on the phase shift in the power curve, they do result in improved model accuracy, with lower C_P values in general and a reduction in the error in C_{Pmax} from 46.9 % to 27 %. As a result, the average RMSE is reduced from 0.155 for the Basic BEMT to 0.121 for BEMT-ALL.

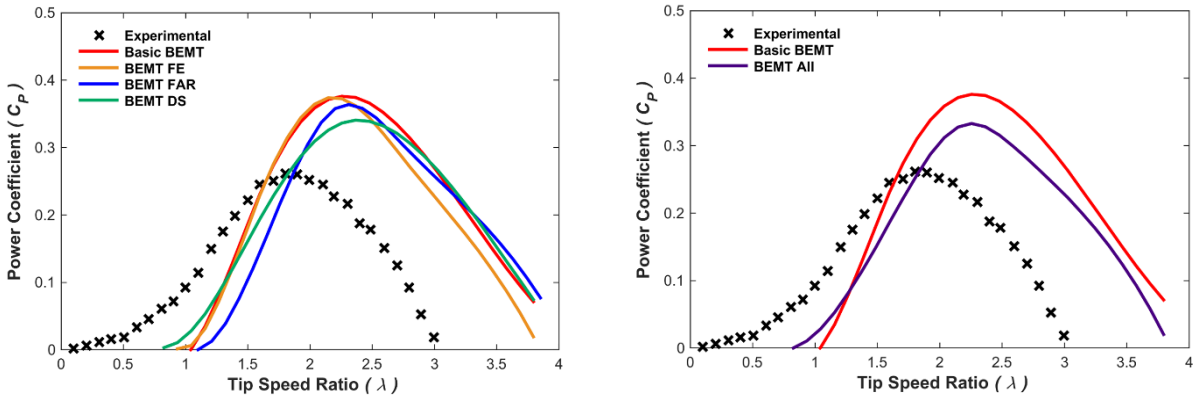

(a) (b)

Figure 16: Comparison of BEMT modelled C_P with measured data [52] for the high solidity VATT.

Table 4: RMSE values for performance prediction of BEMT model for high and low solidity rotors.

	C_P RMSE	
	Low Solidity	High Solidity
Basic BEMT	0.079	0.155
BEMT-FE	0.068	0.140
BEMT-FAR	0.083	0.148
BEMT-DS	0.054	0.137
BEMT-ALL	0.034	0.121

3.2. High Solidity Wind Turbine

The final model with all flow phenomena corrections included was utilsed to predict the performance of a high solidity VAWT in unconfined flow. As before, the model outputs were compared to experimental test data collected by McLaren [53]; details of the turbine are presented in Table 5. The comparison of modelled and measured performance coefficients are shown in Figure 17. The model predicts the general shape of the performance curve quite well with the predicted and measured peak performances occurring at the same tip-speed ratio of 1.8. However, the model over-predicts performance across the entire range of tip-speed ratios. Comparing the median value of measured $C_{\mathrm{P}max}$ of 0.312 and the value including the maximum experimental error of 0.365 with the modelled $C_{\mathrm{P}max}$ value of 0.376, the relative differences are 18.6 % and 5.6 % respectively. These results represent a significant improvement in model performance over the case of the high solidity VATT in confined flow.

Table 5: Details of the high solidity VAWT used to assess model accuracy.

Blades N_B	Turbine Type	Diameter D (m)	Chord-length c (m)	Blade Length L_B (m)	Foil Profile	Solidity σ
3	Wind	2.8	0.42	3	NACA 0015	0.14

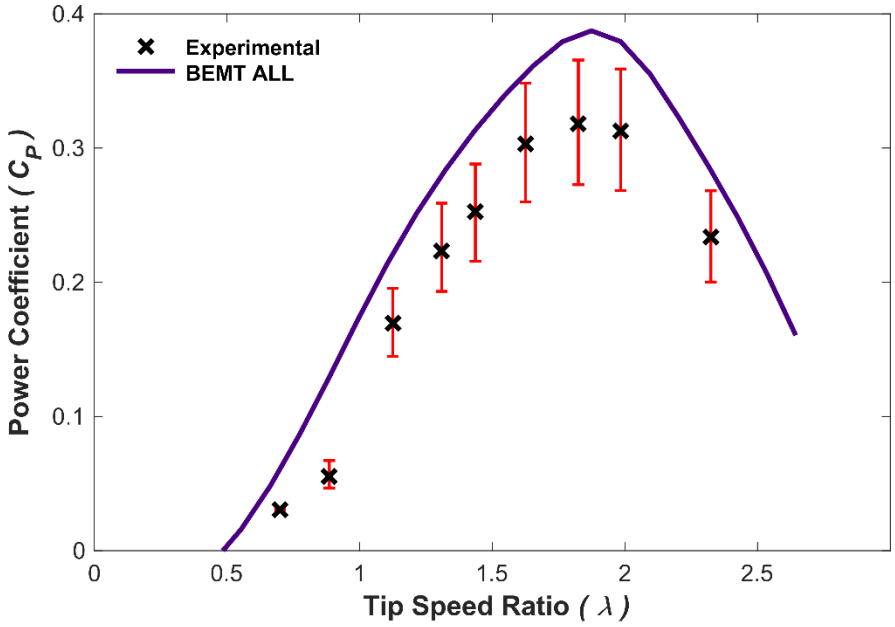

Figure 17: Comparison of BEMT modelled C_{P} with measured data [53] for the high solidity VAWT.

3.3. Strut Effects

To evaluate the effects of the correction for support struts on turbine performance, the model with all flow phenomena corrections and the strut correction was run for all three of the case study turbines. Figure 18 compare the modelled power curves with and without the strut correction to the respective measured power curve data. Similar to the findings of the previous works of Mannion et al. [12] and Kirke and Paillard [48], the struts are shown to have a parasitic effect on power performance which increases with tip-speed ratio. In the absence of the strut correction the BEMT model overpredicts power performance and accuracy is therefore much improved when the parasitic strut effects are accounted for. This was observed for all three turbine studies. For the low solidity wind turbine (Figure 18 (a)), the error in modelled $C_{\mathrm{P}max}$ reduced from 6.4 % to 2.5 %, for the high solidity tidal turbine (Figure 18 (b)) the error reduced from 27 % to 10.2 % and for the high solidity wind turbine (Figure 18 (c)) it reduced from 21.8 % to 8 %. The strut correction also had some effect on the phase shift observed in the model results for the high solidity tidal turbine where the portion of the curve for $\lambda > \lambda_{opt}$ was shifted toward lower tip-speed ratios to give closer agreement with the measured data; however, that portion of the curve for $\lambda > \lambda_{opt}$ was unaffected.

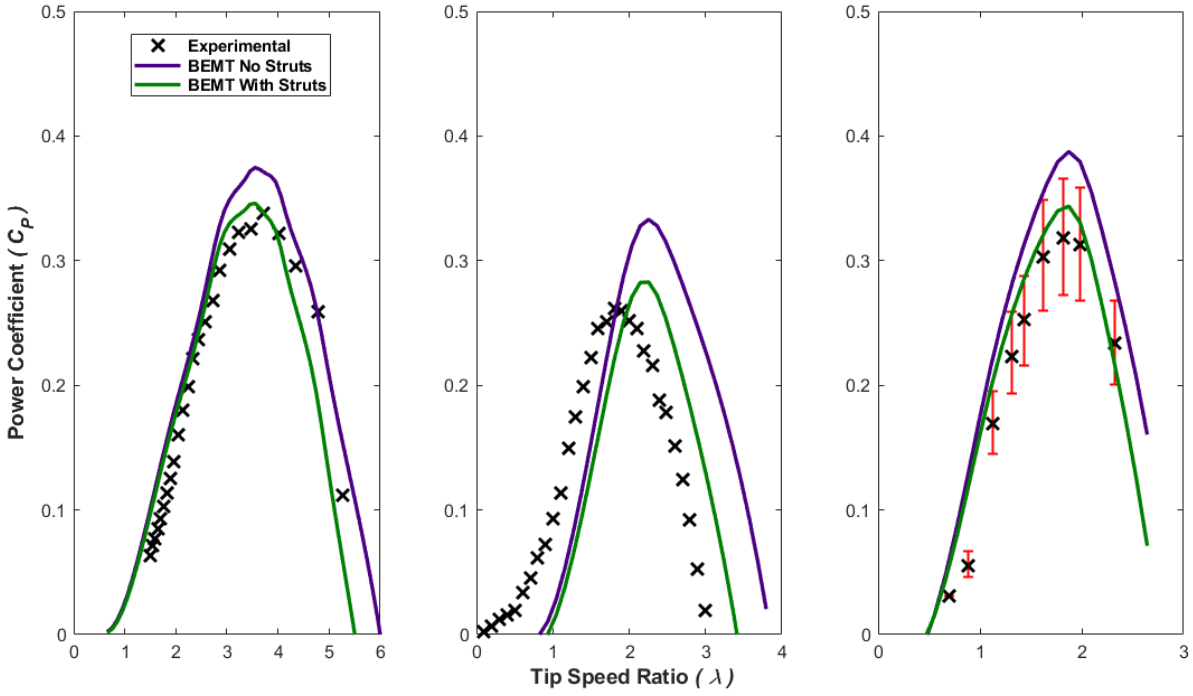

Figure 18: Comparison of BEMT modelled C_{P} with experimental data showing the effects of the support struts for the three turbines: (a) low solidity wind turbine (b) high solidity tidal turbine and (c) high solidity wind turbine.

4. Discussion

This research presents the development and assessment of a bespoke BEMT model to predict the performance of both low and high solidity VAT rotors which is applicable to both wind and tidal turbines. BEMT models are extremely attractive to early-stage developers due to their suitability for rapid evaluation of design iterations. They are much more cost-effective than experimental testing and significantly less computationally expensive than other numerical

modelling techniques such as CFD or vortex models.

This research outlines the model development with a particular focus on the novel contributions contained within the model. The model uses a graphical approach for determining induction factors which makes it suitable for application to high solidity rotors and, to the author's knowledge, this is the first time this approach has been applied to vertical axis tidal turbines. For a VAT, Reynolds number can vary significantly around the azimuthal rotation, and the developed BEMT model captures this by recalculating Reynolds numbers for each location and for every potential induction factor. Correction factors for flow expansion, finite aspect ratio correction and dynamic stall are implemented in the model and can be switched on and off as desired.

BEMT model performance was evaluated for both low solidity and high solidity turbine rotors by comparison with published experimental data. For both low and high solidity rotors, the inclusion of the dynamic stall model had the most significant effect on improving model accuracy. In relation to the low solidity rotor results, the model was shown to be accurate in predicting power performance with an average RMSE of just 0.034 when corrections for flow expansion, finite aspect ratio and dynamic stall were applied simultaneously and a difference in $C_{\mathrm{P}max}$ of just 6.4 %. For the high solidity tidal case, model prediction was less accurate. Most significantly, a phase shift was present in the predicted BEMT power curves compared to the measured curve. An additional study of a high solidity rotor in unconfined flow, showed that this phase shift is likely the result of 3D effects that are not accounted for in the BEMT model, such as blockage effects in the confined tank. In all three turbine studies the BEMT model overpredicted the power performance; a correction for the parasitic effects of support struts was therefore included in the model and was found to further improve model accuracy; in particular, it reduced the predicted power performance across all the full ranges of tip-speed ratios. For the low solidity wind turbine case the error in predicted $C_{\mathrm{P}max}$ was reduced from 6 % to 3 % while for the high solidity tidal and wind turbines the errors were reduced from 27 % to 10 % and from 22 % to 8 %, respectively.

Applications of BEMT models to high solidity rotors, in particular tidal turbines, are rare in the literature. This is due to fact that for high solidity applications, the iterative approach to calculation of induction factors experiences convergence issues [53] which causes model failure. For this reason, BEMT models are largely overlooked as a means of modelling high solidity rotors. It is therefore not possible to conclusively say whether the presented level of accuracy is acceptable for early assessment of a high solidity VATT. However, as a comparison, Li and Calisal [54] overpredicted peak perforamnce of a VATT by 20 % (approximately) using the more computationally-intensive vortex model approach. The presented model therefore shows definite promise in predicting the performance of high solidity turbines and merits further investigation.

5. Conclusions

Numerical models are of vital importance to the development process of commercial-scale tidal (and wind) turbines as they offer a cost-effective alternative to experimental testing for assessment and optimisation of prototypes at any scale. BEMT models can be used in the first instance to estimate the performance of devices and determine blade forces to inform structural design. In the present research a double multiple stream-tube BEMT model has been developed for VATs which uses a graphical approach for determination of induction factors, rather than the traditional iterative approach. The model performance was assessed against experimental

data for both low solidity and high solidity rotors. A complete model description has been presented with details of corrective approaches which are included for dynamic stall, finite aspect ratio blades and flow expansion. The following conclusions are drawn from the research.

- The presented research successfully implemented the graphical approach for determination of induction factors for both low and high solidity rotors. The research shows that this graphical method can be successfully used for high solidity and high loaded rotors, where the iterative approach fails.

- The model was highly accurate when used to predict the performance of a low solidity wind turbine. It reproduced the phase and magnitudes of the power curve with an error in peak power coefficient of just 2.5 %. The model is therefore highly suited to modelling of low solidity VATs.

- The model was less accurate when used to simulate the performance of a high solidity tidal turbine in confined flow. A phase shift was present in the modelled power curve at lower tip-speed ratios and the error in peak power coefficient was 10 %. The absence of a phase shift in the power curve predicted by the model for another high solidity rotor in unconfined flow, suggests that the phase shift is the result of 3D effects that are not accounted for in the BEMT model, such as dynamic stall or blockage effects in the confined tank. Model accuracy could possibly be further improved by incorporating a more complex dynamic stall model, such as a Leishman-Beddoes, or similar. Additionally, the use of a different aerofoil characteristic database to that used here (i.e. Shedahl and Klimas) might also further improve accuracy.

- The flow-related corrective approach which had the greatest effect on model accuracy was the inclusion of the dynamic stall model. It's inclusion reduced the RMSE values for the modelled power curve from 0.079 to 0.054 for the low solidity wind turbine case and from 0.155 to 0.137 for the high solidity tidal turbine case. It is therefore recommended that all VAT BEMT models should include a dynamic stall model.

- The omission of strut effects in BEMT models can lead to significant performance overprediction, it was shown in this research that accounting for these effects can greatly improve model accuracy . Prediction error of experimental data reduced from 6.4 % to 2.5 %, 27 % to 10.2 % and from 21.8 % to 8 % for the investigated scenarios. It is therefore recommended that all VAT BEMT models should include strut effects.

Acknowledgements

This material is based upon works supported by Science Foundation Ireland under Grant No. 12/RC/2302 through MaREI, the national centre for Marine and Renewable Energy Ireland. The authors would also like to thank Dr Simon McIntosh for providing guidance and assistance at the early stages of model development.

Nomenclature

Symbol	Definition	Unit
t_c	Aero/hydrofoil Thickness	m
U_∞	Ambient/Free-stream Velocity	m/s
α	Angle of Attack	deg (∘)
A	Area	m^2
AR	Aspect Ratio	
Q_{avg}	Average Torque	Nm
a	Axial Induction Factor	
θ	Azimuthal Position	deg (∘)
AR	Blade Aspect Ratio	
$C_{x,BET}$	Blade Element Force Coefficient	
L_B	Blade Length	m
ΩR	Blade Tip Speed	m rad/s
x, y, z	Cartesian Coordinates	m
$\Delta\theta$	Change in Azimuthal Position	deg (∘)
Δt	Change in Time/Time-Step	s
c	Chord Length	m
ρ	Density	Kg/m^3
V_d	Downstream-stream Velocity	m/s
C_D	Drag Coefficient	
F_D	Drag Force	N
q	Dynamic Pressure	Pa
V_e	Equilibrium Velocity	m/s
$\tilde{c}$	Equivalent Chord Length	m
F	Force	N
C_x	Force Coefficient	
V_a	Induced Velocity	m/s
Q_i	Instantaneous Torque	Nm
C_L	Lift Coefficient	
F_L	Lift Force	N
Ma	Mach Number	
m	Mass	kg
$\dot{m}$	Mass Flow Rate	kg/s
C_m	Moment Coefficient	
$C_{x,MOM}$	Momentum Force Coefficient	
C_N	Normal Coefficient	
F_N	Normal Force	N
N_B	Number of Blades	
N_tubes	Number of Stream-tubes	

C_{P}	Power Coefficient	
P, p	Pressure	Pa
V_{rec}	Recovered Velocity	m/s
α_{ref}	Reference Angle of Attack	deg (∘)
V_{rel}	Relative Velocity	m/s
Re	Reynolds Number	
σ_{solid}	Solidity	
α_{SS}	Static Stall Angle	deg (∘)
β	Stream-tube Angle	deg (∘)
F_{x}	Stream-wise Force	N
ψ	Strut Angle Relative to Horizontal	deg (∘)
C_{T}	Tangential Coefficient	
F_{T}	Tangential Force	N
T	Thrust	N
$\dot{\alpha}$	Time Derivative Angle of Attack	deg (∘)
λ, TSR	Tip Speed Ratio	
Q	Torque	Nm
R	Turbine Radius	m
Ω	Turbine Rotational Velocity	Rad/s
ε	Turbulent Rate of Dissipation	m^2/s^3
V_u	Upstream Velocity	m/s
u, v, w	Velocities	m/s

Abbreviation	**Definition**
BEM	Blade Element Theory
$BEMT$	Blade Element Momentum Theory
CFD	Computational Fluid Dynamics
$DMST$	Double Multiple Stream-tube
DS	Dynamic Stall
FAR	Finite Aspect Ratio
FE	Flow Expansion
$HATT$	Horizontal Axis Tidal Turbine
HAT	Horizontal Axis Turbine
$HAWT$	Horizontal Axis Wind Turbine
$NACA$	National Advisory Committee for Aeronautics
$RANS$	Reynolds Averaged Navier-Stokes
$RMSE$	Root Mean-Squared Error

RD	Rotor Diameter
$\mathrm{UNH}-\mathrm{RVAT}$	University of New Hampshire Reference Vertical Axis Turbine
$URANS$	Unsteady Reynolds Averaged Navier-Stokes
$VATT$	Vertical Axis Tidal Turbine
VAT	Vertical Axis Turbine
$VAWT$	Vertical Axis Wind Turbine
$2D$	Two-Dimensional
$3D$	Three-Dimensional

Reference

[1] Mannion, B., McCormack, V., Kennedy, C., Leen, S. B., and Nash, S., 2018, "An Experimental Study of a Flow-Accelerating Hydrokinetic Device," Proc. Inst. Mech. Eng. Part A J. Power Energy, p. 095765091877262.

[2] Bachant, P., and Wosnik, M., 2015, "Characterising the Near-Wake of a Cross-Flow Turbine," J. Turbul., **16**(4), pp. 392–410.

[3] Shiono, M., Suzuki, K., and Kiho, S., 2000, "Experimental Study of the Characteristics of a Darrieus Turbine for Tidal Power Generation," Electr. Eng. Japan (English Transl. Denki Gakkai Ronbunshi), **132**(3), pp. 38–47.

[4] Shiono, M., Suzuki, K., and Kiho, S., 2002, "Output Characteristics of Darrieus Water Turbine with Helical Blades for Tidal Current Generations," *Proceedings of the International Offshore and Polar Engineering Conference*, pp. 859–864.

[5] Coiro, D. P., Marco, a De, Nicolosi, F., Melone, S., and Montella, F., 2005, "Dynamic Behaviour of the Patented Kobold Tidal Current Turbine : Numerical and Experimental Aspects," Acta Polytech., **45**(3), pp. 77–84.

[6] Gracie-Orr, K., Nevalainen, T. M., Johnstone, C. M., Murray, R. E., Doman, D. A., and Pegg, M. J., 2016, "Development and Initial Application of a Blade Design Methodology for Overspeed Power-Regulated Tidal Turbines," Int. J. Mar. Energy, **15**, pp. 140–155.

[7] Sun, Z., Chen, J., Shen, W. Z., and Zhu, W. J., 2016, "Improved Blade Element Momentum Theory for Wind Turbine Aerodynamic Computations," Renew. Energy, **96**, pp. 824–831.

[8] Allsop, S., Peyrard, C., Thies, P. R., Boulougouris, E., and Harrison, G. P., 2017, "Hydrodynamic Analysis of a Ducted, Open Centre Tidal Stream Turbine Using Blade Element Momentum Theory," Ocean Eng., **141**(June), pp. 531–542.

[9] Masters, I., Chapman, J. C., Willis, M. R., and Orme, J. A. C., 2011, "A Robust Blade Element Momentum Theory Model for Tidal Stream Turbines Including Tip and Hub

Loss Corrections," J. Mar. Eng. Technol., **10**(1), pp. 25–35.

[10] Wood, D. H., and Okulov, V. L., 2017, "Nonlinear Blade Element-Momentum Analysis of Betz-Goldstein Rotors," Renew. Energy, **107**, pp. 542–549.

[11] Mannion, B., McCormack, V., Leen, S. B., and Nash, S., 2019, "A CFD Investigation of a Variable-Pitch Vertical Axis Hydrokinetic Turbine with Incorporated Flow Acceleration," J. Ocean Eng. Mar. Energy, **5**(1), pp. 21–39.

[12] Mannion, B., Leen, S. B., and Nash, S., 2018, "A Two and Three-Dimensional CFD Investigation into Performance Prediction and Wake Characterisation of a Vertical Axis Turbine," J. Renew. Sustain. Energy, **10**(3), p. 34503.

[13] H. Glauert, 1926, *The Elements of Airfoil and Airscrew Theory*, University Press, Cambridge England.

[14] Templin, R. J., 1974, "Aerodynamic Performance Theory for the NRC Vertical-Axis Wind Turbine," NASA STI/Recon Tech. Rep. N 7616618, **76**, p. 16618.

[15] Strickland, J., 1975, "The Darrieus Turbine, A Performance Prediction Method Using Multiple Stream Tubes," Sandia Lab. SAND, (SAND75-0431).

[16] Paraschivoiu, I., 1988, "Double-Multiple Streamtube Model for Studying VAWT's," J. Propuls. Power, **4**(4), pp. 370–378.

[17] Paraschivoiu, I., 1982, "Aerodynamic Loads and Performance of the Darrieus Rotor," J. Energy, **6**(6), pp. 406–412.

[18] Read, S., and Sharpe, D. J., 1980, "An Extended Multiple Streamtube Theory for Vertical Axis Wind Turbines," *Wind Energy Workshop*, Cranfield, pp. 65–72.

[19] Klimas, P. C., and Sheldahl, R. E., 1978, *"Four Aerodynamic Prediction Schemes for Vertical-Axis: A Compendium," Sandia National Laboratories, Springfield, pp. 1–20.*

[20] Paraschivoiu, I., Delclaux, F., Fraunié, P., and Béguier, C., 1983, "Aerodynamic Analysis of the Darrieus Wind Turbines Including Secondary Effects," J. Energy, **7**(5), pp. 416–422.

[21] Gupta, S., and Leishman, J. G., 2005, "Comparison of Momentum and Vortex Methods for the Aerodynamic Analysis of Wind Turbines," 43rd AIAA Aerosp. Sci. Meet. Exhib., **AIAA 2005**-(January), pp. 1–24.

[22] McIntosh, S. C., Babinsky, H., and Bertenyi, T., 2009, "Convergence Failure and Stall Hysteresis in Actuator-Disk Momentum Models Applied to Vertical Axis Wind Turbines," J. Sol. Energy Eng., **131**(3), p. 034502.

[23] Paraschivoiu, I., Fraunie, P., and Beguier, C., 1985, "Streamtube Expansion Effects on the Darrieus Wind Turbine," J. Propuls. Power, **1**(2), pp. 150–155.

[24] Tsang, K. K. Y., So, R. M. C., Leung, R. C. K., and Wang, X. Q., 2008, "Dynamic Stall Behavior from Unsteady Force Measurements," J. Fluids Struct., **24**(1), pp. 129–150.

[25] Paraschivoiu, I., 2002, *Wind Turbine Design with Emphasis on Darrieus Concept*, Polytechnic international Press.

[26] Gormont, R. E., 1973, “A Mathematical Model of Unsteady Aerodynamics and Radial Flow for Application to Helicopter Rotors,” USAAMRDL Tech. Rep. 72-67, pp. 1–150.

[27] Massé, B., 1981, “Description de Deux Programmes d’ordinateur Pour Le Calcul Des Performance et Des Charges Aérodynamiques Pour Les Éoliennes à Axe Vertical,” Inst. Rech. l’Hydro, **IREQ-2379**.

[28] Berg, D. E., 1983, “Improved Double-Multiple Streamtube Model for the Darrieus-Type Vertical-Axis Wind Turbine,” *Sixth Biannual Wind Energy Conference and Workshop*, Minneapolis.

[29] Beddoes, T. S., 1983, “Representation of Airfoil Behaviour,” Vertica, **7**(2), pp. 183–197.

[30] Leishman, J. G., and Beddoes, T. S., 1989, “A Semi-Empirical Model for Dynamic Stall,” J. Am. Helicopter Soc., **34**(3), pp. 3–17.

[31] Dyachuk, E., and Goude, A., 2015, “Simulating Dynamic Stall Effects for Vertical Axis Wind Turbines Applying a Double Multiple Streamtube Model,” Energies, **8**(2), pp. 1353–1372.

[32] Sheldahl, R. E., and Klimas, P. C., 1981, “Aerodynamic Characteristics of Seven Symmetrical Airfoil Sections through 180-Degree Angle of Attack for Use in Aerodynamic Analysis of Vertical Axis Wind Turbines. Technical Report SAND80-2114, Sandia National Laboratories,” Tech. SAND80-2114, Sandia Natl. Lab.

[33] Abbott, I. H., and Von Doenhoff, A. E., 1959, *Theory of Wing Sections: Including a Summary of Airfoil Data*, Dover Publications, INC. New York.

[34] Viterna, L., and D. Corrigan, R., 1981, “Fixed Pitch Rotor Performance of Large Horizontal Axis Wind Turbines,” *DOE/NASA Workshop on Large Horizontal Axis Wind Turbines*, Cleveland, OH.

[35] Castelli, M. R., Fedrigo, A., and Benini, E., 2012, “Effect of Dynamic Stall, Finite Aspect Ratio and Streamtube Expansion on VAWT Performance Prediction Using the BE-M Model,” World Acad. Sci. Eng. Technol., **68**(8), pp. 426–438.

[36] Soraghan, C. E., 2014, “Aerodynamic Modelling and Control of Vertical Axis Wind Turbines,” University of Strathclyde.

[37] Ferreira, C. S., 2009, “The near Wake of the VAWT 2D and 3D Views of the VAWT Aerodynamics,” Delft University of Technology.

[38] Burton, T., Jenkins, N., Sharpe, D., and Bossanyi, E., 2011, *Wind Energy Handbook, Second Edition*, John Wiley & Sons, Ltd. West Sussex, England.

[39] Freris, L. L., 1990, *Wind Energy Conversion Systems*, Prentice Hall, New York.

[40] White, F., 2010, “Fluid Mechanics,” McGraw-Hill,New York, p. 862.

[41] Masson, C., Leclerc, C., and Paraschivoiu, I., 1998, “Appropriate Dynamic-Stall Models for Performance,” Int. J. Rotating Mach., **4**(2), pp. 129–139.

[42] Lewis, M., Neill, S. P., Robins, P., Hashemi, M. R., and Ward, S., 2017, “Characteristics

of the Velocity Profile at Tidal-Stream Energy Sites," Renew. Energy, **114**, pp. 258–272.

[43] McIntosh, S. C., 2009, "Wind Energy for the Built Environment," University of Cambridge.

[44] Eppler, R., and Somers, D. M., 1980, "A Computer Program for the Design and Analysis of Low-Speed Airfoils," NASA Technical Memorandum 80210.

[45] Antheaume, S., Maître, T., and Achard, J. L., 2008, "Hydraulic Darrieus Turbines Efficiency for Free Fluid Flow Conditions versus Power Farms Conditions," Renew. Energy, **33**(10), pp. 2186–2198.

[46] Wosnik, M., Bachant, P., Neary, V. S., and Murphy, A. W., 2016, "Evaluation of Design & Analysis Code , CACTUS , for Predicting Cross-Flow Hydrokinetic Turbine Performance," SANDIA REPORT SAND2016-9787.

[47] Coiro, D., Montella, F., and Melone, S., 2005, "FLOW CURVATURE EFFECTS ON DYNAMIC BEHAVIOUR OF A NOVEL VERTICAL AXIS TIDAL CURRENT TURBINE: NUMERICAL AND EXPERIMENTAL ANALYSIS," *International Conference on Offshore Mechanics and Arctic Engineering*, pp. 1–9.

[48] Kirke, B. K., and Paillard, B., 2016, "Predicted and Measured Performance of a Vertical Axis Wind Turbine with Passive Variable Pitch Compared to Fixed Pitch," Wind Eng., **41**(1), pp. 1–17.

[49] Hoerner, S. F., 1965, "Fluid Dynamic Drag," Publ. by author, p. 455.

[50] De Marco, A., Coiro, D. P., Cucco, D., and Nicolosi, F., 2014, "A Numerical Study on a Vertical-Axis Wind Turbine with Inclined Arms," Int. J. Aerosp. Eng., **2014**.

[51] Mays, I., Morgan, M., Anderson, M., and Powles, S., 1990, "Experience with the VAWT 850 Demonstration Project," *European Community Wind Energy Conference 1990*, Madrid, Spain, pp. 482–487.

[52] Bachant, P., and Wosnik, M., 2016, "Effects of Reynolds Number on the Energy Conversion and Near-Wake Dynamics of a High Solidity Vertical-Axis Cross-Flow Turbine," Energies, **9**(2), pp. 1–18.

[53] McLaren, K., 2011, "A Numerical and Experimental Study of Unsteady Loading of High Solidity Vertical Axis Wind Turbines," McMaster University.

[54] Li, Y., and Calisal, S. M., 2010, "Three-Dimensional Effects and Arm Effects on Modeling a Vertical Axis Tidal Current Turbine," Renew. Energy, **35**(10), pp. 2325–2334.